Robust Student's t-Based Cooperative Navigation for Autonomous Underwater Vehicles

Qian Li, Yueyang Ben, Syed Mohsen Naqvi, *Senior Member, IEEE*, Jeffrey A. Neasham, and Jonathon A. Chambers, *Fellow, IEEE*

***Abstract*— A robust leader–slave cooperative navigation (CN) algorithm for autonomous underwater vehicles (AUVs) based on the Student's t extended Kalman filter (SEKF) is proposed. Compared with the conventional EKF based on a Gaussian distributed noise assumption, which has been widely used in the field of CN, the Student's t-based filtering algorithms show an improved robustness against outliers existing in the process and measurement noises. The utilization of the Student's t distribution can minimize the negative effect induced by the outliers existing in the underwater acoustic communication system and the cheap but unreliable dead reckoning sensors equipped on the slave AUVs. After a detailed derivation of the robust CN algorithm based on the SEKF, two approximation methods that are required in the Student's t-based filter are discussed and compared. Simulation results show the efficiency and superiority of the robust SEKF-based leader–slave CN algorithm as compared with the conventional EKF-based CN algorithm. The validity of the proposed CN algorithm is also evaluated on field trial data, and the performance of different degrees of freedom (DOF) values, which determine the tail behavior of the Student's t distribution is compared and analyzed, and then the link between the DOF value and the robust effect of the Student's t distribution is revealed, which will act as a guide when applying the Student's t-based filter in the field of CN.**

***Index Terms*— Autonomous underwater vehicle (AUV), cooperative navigation (CN), filtering, outlier, Student's t distribution, underwater acoustic communication.**

I. Introduction

ACCURATE autonomous underwater vehicle (AUV) navigation is a vital enabler for AUV autonomy, and it is also essential to improve the efficiency of AUV missions. Without a global navigation satellite system (GNSS) signal as an external reference underwater, an AUV has to rely on proprioceptive information, obtained through a compass, a Doppler velocity log (DVL) or an inertial navigation system, and a pressure depth sensor to calculate a dead reckoning (DR) navigation solution by integrating velocities, attitude, and pressure depth [1]. Unfortunately, the positioning errors grow unbounded with time based on DR information, independent of the accuracy of the equipped sensors [2], [3]. In order to achieve bounded-error positioning, additional information to correct the positioning error is necessary from an absolute georeferenced source. The most common position correction method underwater is a time-of-flight (TOF) acoustic positioning system, such as an ultrashort baseline (USBL), an SBL, or a long baseline (LBL) approach [4]. Although these systems can localize an AUV underwater, they do not always scale well. For example, the LBL system provides the highest accuracy, but it requires external fixed reference transponders that limit the navigable range of the AUV to 5–10 km. Moreover, it requires a substantial deployment effort before operations, especially in deep water, which is costly and time-consuming.

Recently, multiple AUVs deployment is becoming more common as the technologies upon which the individual AUV relies become more stable and the underwater acoustic communication technique that they use to share commands and information is standardized [5]. Aiming at the deployment of multiple AUVs, cooperative navigation (CN) is a viable option for high-accuracy underwater navigation of multiple AUVs. In a CN system, a fleet of AUVs exchange relative position measurements from their exteroceptive sensors and their motion information from proprioceptive sensors to collectively estimate their states. In [6], it is shown that the rate at which positioning uncertainty increases in a fleet of vehicles is constant, and is identical for all the vehicles in the absence of absolute position measurements. The rate of uncertainty increase is smaller than the best rate any single vehicle would attain, if it was localizing on its own. The study indicates that the exchange of positioning information benefits all vehicles. Furthermore, if absolute georeference information could be provided to one of the vehicles, the states of vehicles performing CN are observable in a connected relative position measurement graph [7]. That is to say, if one vehicle functions similar to a beacon of an acoustic positioning system, the rate at which positioning uncertainty increases in the fleet of AUVs is low or even bounded. More importantly, this vehicle is not static and does not require a substantial deployment effort

Manuscript received September 8, 2017; revised January 21, 2017; accepted January 22, 2017. Date of publication March 29, 2018; date of current version July 12, 2018. This work was supported in part by the National Natural Science Foundation of China under Grant 51509063 and Grant 61503090, in part by the China Post-Doctoral Science Foundation under Grant 2015M81440, in part by the Fundamental Research Funds for the Central Universities under Grant HIT. MKSTISP. 201603 and Grant HIT. NSRIF. 201813, and in part by the Heilongjiang Provincial Natural Science Foundation under Grant QC2013C069. The Associate Editor coordinating the review process was Dr. Amitava Chatterjee. *(Corresponding author: Qian Li.)*

Q. Li is with the Department of Electrical Engineering and Automation, Harbin Institute of Technology, Harbin 150001, China, and also with the Department of Automation, Harbin Engineering University, Harbin 150001, China (e-mail: liqianheu@163.com).

Y. Ben is with the Department of Automation, Harbin Engineering University, Harbin 150001, China (e-mail: byy@hrbeu.edu.cn).

S. M. Naqvi and J. A. Neasham are with the Intelligent Sensing and Communication Group, School of Engineering, Newcastle University, Newcastle upon Tyne NE1 7RU, U.K. (e-mail: mohsen.naqvi@newcastle.ac.uk; jeff.neasham@newcastle.ac.uk).

J. A. Chambers is with the Department of Automation, Harbin Engineering University, Harbin 150001, China, and also with the Intelligent Sensing and Communication Group, School of Engineering, Newcastle University, Newcastle upon Tyne NE1 7RU, U.K. (e-mail: jonathon.chambers@newcastle.ac.uk).

Color versions of one or more of the figures in this paper are available online at http://ieeexplore.ieee.org.

Digital Object Identifier 10.1109/TIM.2018.2809139

before operating as the static beacon in the acoustic positioning system. In addition, this vehicle could be either a mobile surface vehicle with permanent access to a GNSS signal, or an AUV with a very expensive and accurate navigation suite. Therefore, this kind of AUV or mobile surface vehicle can be regarded as a leader or master. Once the other AUVs equipped with low-accuracy DR sensors receive information from the leader or master AUV, they combine the information with their own DR information within an estimation framework to improve their position estimates. Such increase in navigation accuracy is a major benefit to a CN system, and its advantages also include sensor coverage, robustness, efficiency, and flexibility, and thus it remains an active area of research [8], [9].

CN algorithms for multiple AUVs fall within the broader problem of multirobot cooperative localization which has been studied in great depth, and many CN algorithms that could make a consistent and accurate estimation of the positions for a group of robots have been proposed [10]–[13]. Estimation algorithms and techniques, such as the extended Kalman filter (EKF) [14], minimum mean-square estimator [15], maximum likelihood estimator [16], particle filter [17], and maximum *a posteriori* estimator [18], have been used to enhance CN. No matter whether they are used in a centralized [19] or in a decentralized manner [14], these algorithms inevitably face unique constraints in a CN system for multiple AUVs, such as the problem of low data rates and high latency induced by underwater acoustic communication. Some CN algorithms have been proposed to cope with the problem of low data rates and high latency in the CN system for multiple AVUs [20]–[22]. However, most CN algorithms proposed for an AUV CN system assume that the states and measurements are distributed normally around the true mean, namely, a Gaussian distribution. In practical engineering, the underwater acoustic communication system and the cheap but unreliable DR sensors present on slave AUVs could both induce some outliers, which are far away from the true mean [23], [24]. Therefore, the Gaussian distribution assumptions of the process and measurement noises are violated by these outliers. Correspondingly, even a single occasional outlier will potentially introduce a significant bias in a Gaussian distributed filter, such as a conventional KF or EKF estimate, leading to an unacceptably long period of time for reconvergence of the estimated AUV position. Some different variations of the KF have been proposed to deal with outliers in the field of integrated navigation. The most common way to remove outliers is setting a rejection threshold. In [25], two different approaches are presented to reject outliers of the LBL range data: travel time rejection and fix rejection. In [23], the approach proposed for identifying outliers in the range measurement is to represent a set of measurements as a graph, and apply graph partitioning algorithms to identify sets of consistent measurements. However, simply using a rejection threshold is not a good way to eliminate them, since this method can cause the measurement weights to jump from the original value to zero if the measurement errors are located near both sides of the threshold. Moreover, this method requires manual parameter tuning or heuristic parameter estimation procedures [26].

In fact, such outliers can be modeled by a distribution that has heavier tails. Olson *et al.* [23] have shown that the noise in the TOF ranging measurements does not have a Gaussian distribution and signal reflections from the surface of the water as well as from temperature or salinity discontinuities within the water column itself lead to a distribution which is heavy-tailed [27]. Therefore, applying the Student's t distribution that has heavier tails to model the noise in the CN system for multiple AUVs to mitigate the outliers is reasonable. Some Student's t-based filtering algorithms have been proposed for coping with heavy-tailed noise including outliers in the signal processing community. Earlier efforts to derive filters based on the Student's t distribution are represented in [28] and [29] but did not receive much attention. Some linear approaches for realizing filters have been derived based on the variational Bayesian approach to solve the filtering problems of linear systems with heavy-tailed measurement noise [26], [30], [31]. In addition, nonlinear systems with additive noise, Gaussian state transition, and Student's t measurement noise are studied in [32] and [33] where a variational Bayesian approach is also employed. However, these filtering algorithms are not suitable for the case of heavy-tailed process noise since they are all based on the assumption of well-behaved process noise admitting a Gaussian distribution.

With the assumption that both the process noise and measurement noise admit a Student's t distribution, a robust Student's t filter for a linear system is derived by approximating the posterior probability density function (pdf) as a Student's t distribution, and the process noise and measurement noise are both assumed to have Student's t distributions [34]. Huang *et al.* [35] proposed a third-degree Student's t spherical-radial cubature rule and developed a new robust Student's t-based cubature filter to perform nonlinear estimation when the outliers exist in both process and measurement noises. In [36], an approximate smoother for the case with additive process and measurement noises both adopting a Student's t distribution is also developed using variational Bayes. In [24], a sigma-point method for filtering nonlinear systems where Student's t distributed process and measurement noises enter the system nonadditively is developed in an analogous manner to the unscented KF (UKF). Similar to [24], an unscented transform is used to compute the Student's t weighted integrals to solve the nonlinear filtering problem when the process noise and measurement noise both admit a Student's t distribution [37]. It is evident that Student's t-based filtering algorithms have to some extent already been investigated well. However, to the best of our knowledge, there are few studies about using the Student's t distribution to cope with the outliers induced by the underwater acoustic communication system and unreliable DR sensors equipped on the slave AUVs in a CN system for multiple AUVs. Especially, some details including the approximation step and DOF parameter selection in the Student's t-based filter which will impact the performance of the filter are absent up to now.

Due to the stability issue and the heavy calculation burden as well as other limitations of some advanced nonlinear filters [38], such as UKF and particle filter, EKF-based CN algorithm is more appropriate in practical engineering, and it

has been widely used in the field of CN and many commercial navigation products [39]. Therefore, our objective for this paper is to explore a more practical CN algorithm similar to EKF-based CN algorithm, and it also has an improved robustness against outliers existing in the process and measurement noises. In this paper, therefore, the process and measurement noises contaminated by the outliers from the underwater acoustic communication system and unreliable DR sensors are modeled by a Student's t distribution, and a robust leader–slave CN algorithm for multiple AUVs based on a Student's t EKF (SEKF) is proposed. Both the simulation evaluation and the field trial are performed to demonstrate the feasibility and practicability of this robust SEKF-based CN algorithm. Beyond the development of a robust CN algorithm based on Student's t distribution, the second contribution of this paper is to discuss the two approximation methods required in the Student's t-based filters and to provide a quantitative performance comparison of these two approximation methods. This paper also contributes a discussion of the importance of degrees of freedom (DOF) selection in the practical engineering, then the link between the DOF value and the robust effect of the Student's t-based filtering algorithm is revealed. All in all, this paper can be regarded as a stepping stone in the development of Student's t-based filters, especially for applying in the field of CN.

II. Problem Formulation

In this paper, we define the navigation reference frame (x, y, z) as a local-level frame with three axes pointing east, north, and up, respectively. In a CN system for multiple AUVs, an accurate on-board depth sensor is usually equipped on the salve AUVs, and the depth sensor measurement is an excellent correction source for the z-dimension of the position estimate [4]. Therefore, the 3-D navigation problem is converted into the 2-D navigation problem.

A. System Model

First, we consider a fleet of AUVs formed by m slave AUVs which are all equipped with a low cost but low-accuracy velocity sensor and an orientation sensor, and the velocity and orientation measured by these proprioceptive sensors are propagated periodically to maintain a DR navigation solution. Specifically, the discrete-time kinematic equation on the xy horizontal plane for the ith AUV of the fleet of AUVs can be written as follows:

$$\begin{aligned} x_k^i &= x_{k-1}^i + t \cdot \hat{\upsilon}_k^i \cdot \cos\hat{\theta}_k^i + t \cdot \hat{\omega}_k^i \cdot \sin\hat{\theta}_k^i \\ y_k^i &= y_{k-1}^i + t \cdot \hat{\upsilon}_k^i \cdot \sin\hat{\theta}_k^i - t \cdot \hat{\omega}_k^i \cdot \cos\hat{\theta}_k^i \\ \theta_k^i &= \hat{\theta}_k^i \end{aligned} \tag{1}$$

where the elements of $\mathbf{x}_k^i = [x_k^i, y_k^i, \theta_k^i]^T$ denote the east and north components of the ith AUV position together with its heading angle at time step k, respectively. The parameter t is the DR sampling period. In addition, $\hat{\upsilon}_k^i$ and $\hat{\omega}_k^i$, respectively, denote the forward velocity and the starboard velocity of the ith AUV, and the symbol $(\hat{\cdot})$ denotes the measured value. Generally, the forward velocity and the starboard velocity together with the heading angle, which constitute the control input vector $\mathbf{u}_k^i = (\hat{\upsilon}_k^i, \hat{\omega}_k^i, \hat{\theta}_k^i)^T$ are usually measured by a DVL or an electromagnetic log (EM log) and a compass [2].

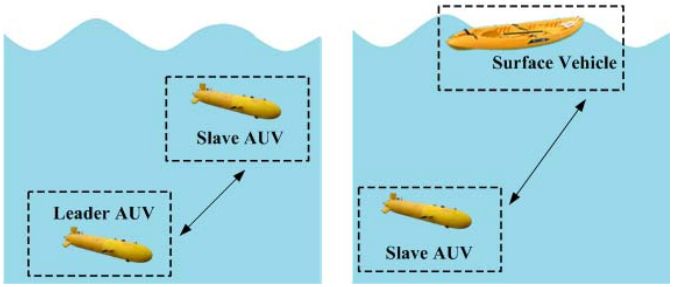

Fig. 1. Configuration of leader–slave CN system for AUVs. Left: one leader AUV and one slave AUV. Right: one mobile surface vehicle and one slave AUV.

To bound the accumulated positioning error of the DR solution in the slave AUVs, one or more leader AUVs that are equipped with high-accuracy navigation suites should support the fleet of slave AUVs. To facilitate the discussion, a classic configuration of two AUVs for CN is shown in Fig. 1. In Fig. 1 (left), there is a slave AUV, which is equipped with a low cost but low-accuracy compass and a DVL or an EM log in the CN system. Typical positioning error with this kind of DR sensors is 20 Nmile/h or even more. To bound the accumulated positioning error of the slave AUV, a leader AUV with a very expensive and accurate navigation suite is included in the CN system as shown in Fig. 1 (left). With the range measurement to the leader AUV and the accurate position of the leader AUV, the unbounded positioning error of the slave AUV can be corrected by a filtering technique. This is a typical framework of leader–slave CN system for AUVs [40]. It is worth mentioning that the leader AUV could be replaced with a mobile surface vehicle with a permanent access to a GNSS signal as shown in Fig. 1 (right), and the function of the mobile surface vehicle is similar to the leader AUV.

Considering the discrete-time kinematic equation for the slave AUV, the process equation of the CN system can be written as follows:

$$\mathbf{x}_k = \mathbf{f}(\mathbf{x}_{k-1}, \mathbf{u}_k, \mathbf{w}_k) \tag{2}$$

where $\mathbf{x}_k = [x_k, y_k, \theta_k]^T$ is the state vector and $\mathbf{w}_k$ is the process noise.

It can be found that the process function $\mathbf{f}(\cdot)$ in (2) is nonlinear according to the discrete-time kinematic equation (1). Therefore, it is necessary to provide the partial derivative matrix to be applied in the SEKF-based CN algorithm proposed in Section III. The partial derivative matrix of the process function is as follows:

$$\mathbf{F}_{\mathbf{x}_k} = \begin{bmatrix} 1 & 0 & -t \cdot \hat{\upsilon}_k \cdot \sin\hat{\theta}_k + t \cdot \hat{\omega}_k \cdot \cos\hat{\theta}_k \\ 0 & 1 & t \cdot \hat{\upsilon}_k \cdot \cos\hat{\theta}_k + t \cdot \hat{\omega}_k \cdot \sin\hat{\theta}_k \\ 0 & 0 & 1 \end{bmatrix} \tag{3}$$

$$\mathbf{F}_{\mathbf{w}_k} = \begin{bmatrix} t \cdot \cos\hat{\theta}_k & t \cdot \sin\hat{\theta}_k & 0 \\ t \cdot \sin\hat{\theta}_k & -t \cdot \cos\hat{\theta}_k & 0 \\ 0 & 0 & 1 \end{bmatrix}. \tag{4}$$

The measurement vector is the range between the leader AUV and the slave AUV, which is represented as follows:

$$\mathbf{z}_k = \sqrt{\left(x_k^l - x_k^s\right)^2 + \left(y_k^l - y_k^s\right)^2} + \mathbf{v}_k \tag{5}$$

where the superscript s and l represent the slave AUV and the leader AUV, respectively. In addition, $\mathbf{v}_k$ is the measurement noise.

Similarly, the measurement equation is nonlinear and its partial derivative matrix is given as

$$\mathbf{H}_k = \begin{bmatrix} \dfrac{\tilde{x}_k^s - \hat{x}_k^l}{r_{ls}} & \dfrac{\tilde{y}_k^s - \hat{y}_k^l}{r_{ls}} & 0 \end{bmatrix} \tag{6}$$

where $r_{ls} = ((\hat{x}_k^l - \tilde{x}_k^s)^2 + (\hat{y}_k^l - \tilde{y}_k^s)^2)^{1/2}$ is the predicted range and $\tilde{x}_k^s$ and $\tilde{y}_k^s$ are the predicted positions of the slave AUV. In addition, $\hat{x}_k^l, \hat{y}_k^l$ are the measured position of the leader AUV transmitted to the slave AUV through the underwater acoustic communication system, and it is regarded as to be accurate.

Equations (2) and (5) constitute the system model of the leader–slave CN system for AUVs.

B. Distribution of Process and Measurement Noises

Now, let us recall the process noise $\mathbf{w}_k$ and the measurement noise $\mathbf{v}_k$ existing in (2) and (5). Most CN algorithms for AUVs assume that the states and measurements are distributed normally around the true mean, namely, the Gaussian distribution. However, for the underwater acoustic communication system, which is the main communication method underwater, this is most certainly not the case. Signal reflections from the surface of the water as well as from temperature or salinity discontinuities within the water column itself lead to outliers existing in the acoustic measurement data. In addition to the outliers existing in the measurement data, due to the unreliability of the DR sensors equipped on the slave AUVs, the process noise may also include outliers. These outliers also violate the Gaussian assumption of the process noise. The outliers existing in the process noise and measurement noise lead to a heavy-tailed distributed noise, rather than a Gaussian distributed noise.

To be more in line with the heavy-tailed behavior induced by the outliers in the process and measurement noises, we introduce the multivariate Student's t distribution to describe the process noise $\mathbf{w}_k$ and the measurement noise $\mathbf{v}_k$ as follows [41]:

$$\mathrm{St}(\mathbf{x}; \hat{\mathbf{x}}, \mathbf{\Sigma}, \nu) = \frac{\Gamma\left(\frac{\nu+n_{dx}}{2}\right)}{\Gamma\left(\frac{\nu}{2}\right)} \frac{1}{(\pi\nu)^{\frac{n_{dx}}{2}} \sqrt{|\mathbf{\Sigma}|}} \times \left(1 + \frac{1}{\nu}(\mathbf{x}-\hat{\mathbf{x}})^T \mathbf{\Sigma}^{-1}(\mathbf{x}-\hat{\mathbf{x}})\right)^{-\frac{n_{dx}+\nu}{2}} \tag{7}$$

where $\Gamma(r) = \int_0^\infty e^{-t} t^{r-1} dr$ is the Gamma function, $\mathbf{x} = [x_1, \ldots, x_{n_{dx}}]^T$ is an n_{dx}-D random vector, ν is the DOF, $\hat{\mathbf{x}}$ is the mean vector, $\mathbf{\Sigma}$ is the symmetric matrix, and $|\cdot|$ represents the determinant operator. Note that the symmetric matrix $\mathbf{\Sigma}$ is not the covariance matrix of the random vector $\mathbf{x}$, and its covariance matrix is related with $\mathbf{\Sigma}$ for $\nu > 2$ as in the following equation [35]:

$$E[(\mathbf{x} - \hat{\mathbf{x}})(\mathbf{x} - \hat{\mathbf{x}})^T] = \frac{\nu}{\nu - 2}\mathbf{\Sigma}. \tag{8}$$

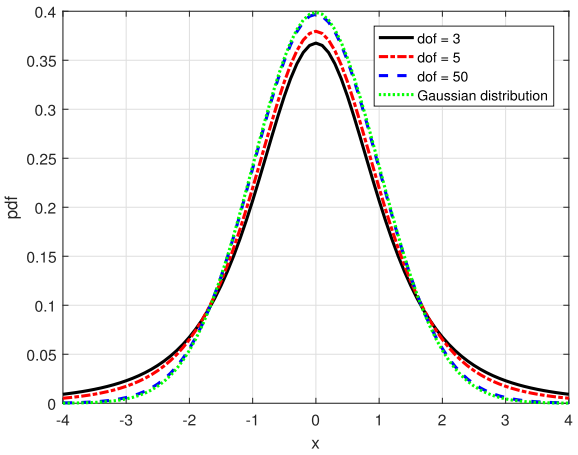

Fig. 2. Comparison of Gaussian distribution (green dotted line) and Student's t distribution with different DOF values ($\nu = 3, 5, 50$).

The DOF ν that determines the tail behavior of the Student's t distribution is an important parameter. When $\nu = 1$, the Student's t distribution reduces to the Cauchy distribution, while in the limit $\nu \to \infty$, the Student's t distribution becomes a Gaussian distribution $\mathcal{N}(\hat{\mathbf{x}}, \mathbf{\Sigma})$. In Fig. 2, the posterior pdf of several Student's t distributions with different DOF values are drawn and compared. It can be seen from Fig. 2 that the Student's t distribution becomes closer to the Gaussian distribution (green dotted line) as the DOF value ν increases, and the tail becomes heavier as the DOF value ν decreases. Therefore, a Student's t distribution with an appropriate DOF value is more in tune with the heavy-tailed behavior of the noise.

In fact, the Student's t distribution can be seen as adding up an infinite number of Gaussian distributions having the same mean but different variances [42]. This distribution, in general, has heavier tails than a Gaussian as a result. This should give algorithms derived on the basis of the Student's t distribution an important property called robustness, which means that they are much less sensitive than those based on a Gaussian assumption to the presence of a few outlier values. In addition, to facilitate the discussion later, another form of Student's t distribution is given here. Let random vector $\mathbf{m} \sim \mathrm{Gam}(\alpha, \beta)$ and $\mathbf{y} \sim \mathcal{N}(\mathbf{0}, \mathbf{\Sigma})$ [42], then $\mathbf{x} = \hat{\mathbf{x}} + \mathbf{m}^{-(1/2)}\mathbf{y}$ admits a Student's t distribution with density as [41]

$$St\left(\mathbf{x}; \hat{\mathbf{x}}, \frac{\beta}{\alpha}\mathbf{\Sigma}, 2\alpha\right) = \frac{\Gamma\left(\alpha + \frac{n_{dx}}{2}\right)}{\Gamma(\alpha)} \frac{1}{(2\beta\pi)^{\frac{n_{dx}}{2}} \sqrt{|\mathbf{\Sigma}|}} \left(1 + \frac{\Delta^2}{2\beta}\right)^{-\frac{n_{dx}}{2}-\alpha} \tag{9}$$

where $\Delta^2 = \left(\mathbf{x} - \hat{\mathbf{x}}\right)^T \mathbf{\Sigma}^{-1}(\mathbf{x} - \hat{\mathbf{x}})$, and it is straightforward to show that (9) turns into (7) for $\alpha = \beta = \nu/2$. The density of

a Gamma distribution $\mathrm{Gam}(\alpha, \beta)$ is represented as follows:

$$\mathrm{Gam}(x;\alpha,\beta) = \begin{cases} \dfrac{\beta^{\alpha}}{\Gamma(\alpha)} x^{\alpha-1} e^{-\beta x}, & x > 0 \\ 0, & \text{otherwise} \end{cases} \tag{10}$$

where $\alpha > 0$ is the shape parameter and $\beta > 0$ is the rate parameter.

III. Cooperative Navigation Algorithm Based on Student's t Distribution

As mentioned in Section II, we use the heavy-tailed Student's t distribution to model the process noise and measurement noise in the CN system for AUVs. Thus, an effective robust CN algorithm should also be designed based on a Student's t distribution.

In this section, we propose a robust CN algorithm based on the SEKF. For a CN system for multiple AUVs, a nonlinear process equation and a measurement equation are usually involved as presented in (2) and (5). Thus, directly porting the linear Student's t filtering algorithm to the CN case is not straightforward. Fortunately, both the Gaussian distribution and the Student's t distribution are closed under linear transformation, thus the framework of linear Student's t filtering algorithm can be extended to nonlinear systems in a manner similar to the development of the EKF for Gaussian systems. Thus, an SEKF that combines the advantage of EKF with the Student's t distribution not only can cope with the outliers but also meets the requirement of computational burden in practical engineering.

A. Student's t Extended Kalman Filtering Algorithm

First, we rewrite the nonlinear process equation and the measurement equation as follows:

$$\begin{aligned} \mathbf{x}_k &= \mathbf{f}(\mathbf{x}_{k-1}, \mathbf{u}_k, \mathbf{w}_k) \\ \mathbf{z}_k &= \mathbf{h}(\mathbf{x}_k, \mathbf{v}_k) \end{aligned} \tag{11}$$

where k denotes the kth time step, $\mathbf{x} \in \mathbb{R}^{n_{dx}}$ is the state vector, $\mathbf{z} \in \mathbb{R}^{n_{dz}}$ is the measurement vector, $\mathbf{f}(\cdot)$ and $\mathbf{h}(\cdot)$ are, respectively, nonlinear process function and measurement function, $\mathbf{w} \in \mathbb{R}^{n_{dx}}$ is the heavy-tailed process noise, and $\mathbf{v} \in \mathbb{R}^{n_{dz}}$ is the heavy-tailed measurement noise. In addition, the process and measurement noises are considered as to be additive.

The initial state and the process and measurement noises are mutually uncorrelated and Student's t distributed with marginal densities as

$$\begin{aligned} p(\mathbf{x}_0) &= \mathrm{St}(\mathbf{x}_0; \hat{\mathbf{x}}_0, \mathbf{\Sigma}_0, \eta_0) \\ p(\mathbf{w}_k) &= \mathrm{St}(\mathbf{w}_k; \mathbf{0}, \mathbf{Q}_k, \gamma) \\ p(\mathbf{v}_k) &= \mathrm{St}(\mathbf{v}_k; \mathbf{0}, \mathbf{R}_k, \delta) \end{aligned} \tag{12}$$

where the DOF values η_0, γ, andδ determine the tail behavior of the related densities.

Similar to the conventional EKF, the SEKF also includes a time update and a measurement update. In the time update, we first assume the DOF for $p(\mathbf{x}_{k-1}|\mathbf{z}_{1:k-1})$ is η_{k-1}, and $\eta_{k-1} = \gamma$ for all k, then we can formulate a joint Student's t density because of the common DOF, i.e., $\eta_{k-1} = \gamma$ as

$$\begin{aligned} &p(\mathbf{x}_{k-1}, \mathbf{w}_{k-1}|\mathbf{z}_{1:k-1}) \\ &\quad = \mathrm{St}\left(\begin{bmatrix} \mathbf{x}_{k-1} \\ \mathbf{w}_{k-1} \end{bmatrix}; \begin{bmatrix} \hat{\mathbf{x}}_{k-1}^{+} \\ \mathbf{0} \end{bmatrix}, \begin{bmatrix} \mathbf{\Sigma}_{k-1}^{+} & \mathbf{0} \\ \mathbf{0} & \mathbf{Q}_{k-1} \end{bmatrix}, \eta_{k-1} = \gamma \right) \end{aligned} \tag{13}$$

where the superscript $^{+}$ denotes the estimated value after seeing the measurement. Thus, $\hat{\mathbf{x}}_{k-1}^{+}$ and $\mathbf{\Sigma}_{k-1}^{+}$ are the estimated state and symmetric matrices, respectively, at time step $k-1$.

Then, we assume that the prediction density is also a Student's t distribution and the DOF η_{k-1} is not changed after nonlinear transformation $\mathbf{f}(\cdot)$. The prediction density can be represented as the following equation:

$$p(\mathbf{x}_k|\mathbf{z}_{1:k-1}) = \mathrm{St}\big(\mathbf{x}_k; \hat{\mathbf{x}}_k^{-}, \mathbf{\Sigma}_k^{-}, \eta_{k-1} = \gamma\big) \tag{14}$$

where the subscript $^{-}$ denotes the predicted value before seeing the measurement.

To calculate the prediction parameters $\hat{\mathbf{x}}_k^{-}$ and $\mathbf{\Sigma}_k^{-}$ in (14), we perform a linearization to the process equation in a manner similar to the development of the EKF for Gaussian systems to obtain the Jacobian matrices of the process equation $\mathbf{F}_{\mathbf{x}_{k-1}} = \partial\mathbf{f}/\partial\mathbf{x}_{k-1}$ and $\mathbf{F}_{\mathbf{w}_{k-1}} = \partial\mathbf{f}/\partial\mathbf{w}_{k-1}$ as shown in (3) and (4). Thus, we can perform the time update of the predicted state and symmetric matrices as follows:

$$\begin{aligned} \hat{\mathbf{x}}_k^{-} &= \mathbf{f}\big(\hat{\mathbf{x}}_{k-1}^{+}, \mathbf{u}_k, \mathbf{0}\big) \\ \mathbf{\Sigma}_k^{-} &= \mathbf{F}_{\mathbf{x}_{k-1}} \mathbf{\Sigma}_{k-1}^{+} \mathbf{F}_{\mathbf{x}_{k-1}}^{T} + \mathbf{F}_{\mathbf{w}_{k-1}} \mathbf{Q}_{k-1} \mathbf{F}_{\mathbf{w}_{k-1}}^{T}. \end{aligned} \tag{15}$$

The result in (15) is guaranteed by the property of the Student's t distributed random vector as follows [41].

Remark 1: If $\mathbf{x}$ has the n_{dx}-variate Student's t distribution with DOF ν, mean vector $\hat{\mathbf{x}}$, and symmetric matrix $\mathbf{\Sigma}$, then, for any nonsingular scalar matrix $\mathbf{C}$ and for any $\mathbf{a}$, $\mathbf{Cx} + \mathbf{a}$ has the n_{dx}-variate Student's t distribution with DOF ν, mean vector $\mathbf{C}\hat{\mathbf{x}} + \mathbf{a}$, and symmetric matrix $\mathbf{C\Sigma C}^{T}$.

This property is of importance in applications and is similar to the corresponding result for the multivariate Gaussian distribution. It is straightforward to find that the time update of the SEKF algorithm is similar to that for the conventional EKF time update.

In the measurement update, we make assumptions on the DOF in the same fashion. For $\eta_{k-1} = \delta$, then we can formulate a joint Student's t density for the predicted state and the measurement noises as follows:

$$\begin{aligned} &p(\mathbf{x}_k, \mathbf{v}_k|\mathbf{z}_{1:k-1}) \\ &\quad = \mathrm{St}\left(\begin{bmatrix} \mathbf{x}_k \\ \mathbf{v}_k \end{bmatrix}; \begin{bmatrix} \hat{\mathbf{x}}_k^{-} \\ \mathbf{0} \end{bmatrix}, \begin{bmatrix} \mathbf{\Sigma}_k^{-} & \mathbf{0} \\ \mathbf{0} & \mathbf{R}_k \end{bmatrix}, \eta_{k-1} = \delta \right). \end{aligned} \tag{16}$$

Similarly, we linearize the measurement equation $\mathbf{h}(\cdot)$ by performing a Taylor series expansion. Then, the joint Student's t density of the state and the measurement vectors is written as

$$\begin{aligned} &p(\mathbf{x}_k, \mathbf{z}_k|\mathbf{z}_{1:k-1}) \\ &= \mathrm{St}\left(\begin{bmatrix} \mathbf{x}_k \\ \mathbf{z}_k \end{bmatrix}; \begin{bmatrix} \hat{\mathbf{x}}_k^{-} \\ \mathbf{h}\left(\hat{\mathbf{x}}_k^{-}, \mathbf{0}\right) \end{bmatrix}, \begin{bmatrix} \mathbf{\Sigma}_k^{-} & \mathbf{\Sigma}_k^{-}\mathbf{H}_k^{T} \\ \mathbf{H}_k\mathbf{\Sigma}_k^{-} & \mathbf{H}_k\mathbf{\Sigma}_k^{-}\mathbf{H}_k^{T} + \mathbf{R}_k \end{bmatrix}, \eta_{k-1} \right) \end{aligned} \tag{17}$$

where the linearized measurement matrix $\mathbf{H}_k = \partial \mathbf{h}/\partial \mathbf{x}_k$ is the Jacobian matrix of the measurement equation as shown in (6).

Then, the conditional density of the estimated state given all measurements $\mathbf{z}_{1:k}$ can be also expressed as a Student's t distribution as follows:

$$p(\mathbf{x}_k|\mathbf{z}_{1:k}) = \mathrm{St}\big(\mathbf{x}_k; \hat{\mathbf{x}}_k^+, \mathbf{\Sigma}_k^+, \eta_k\big). \tag{18}$$

To obtain the posterior parameters of (18), we can calculate the conditional density (18) using (9) as follows:

$$\begin{aligned} &p(\mathbf{x}_k|\mathbf{z}_k) \\ &= \frac{p(\mathbf{x}_k, \mathbf{z}_k)}{p(\mathbf{z}_k)} = \frac{\Gamma\left(\alpha + \frac{n}{2}\right)}{\Gamma(\alpha)} \frac{1}{(2\beta\pi)^{\frac{n}{2}}} \\ &\quad \times \frac{1}{\sqrt{|\mathbf{\Sigma}|}} \left(1 + \frac{\Delta^2}{2\beta}\right)^{-\frac{n}{2}-\alpha} \\ &\quad \times \left(\frac{\Gamma\left(\alpha + \frac{n_{dz}}{2}\right)}{\Gamma(\alpha)} \frac{1}{(2\beta\pi)^{\frac{n_{dz}}{2}}} \frac{1}{\sqrt{|\mathbf{\Sigma}_{22}|}} \left(1 + \frac{\Delta_z^2}{2\beta}\right)^{-\frac{n_{dz}}{2}-\alpha}\right)^{-1} \end{aligned} \tag{19}$$

where $n = n_{dx} + n_{dz}$, $\mathbf{\Sigma}$ is the symmetric matrix of the joint density of the state and the measurement in (17), and $\mathbf{\Sigma}_{ij}(i, j = 1, 2)$ is the ith row and jth column elements of the block matrix $\mathbf{\Sigma}$. In addition, the quadratic form Δ_z^2 is defined as

$$\Delta_z^2 = \big(\mathbf{z}_k - \mathbf{h}\big(\hat{\mathbf{x}}_k^-, \mathbf{0}\big)\big)^T \mathbf{\Sigma}_{22}^{-1} \big(\mathbf{z}_k - \mathbf{h}\big(\hat{\mathbf{x}}_k^-, \mathbf{0}\big)\big). \tag{20}$$

After derivation, the conditional density $p(\mathbf{x}_k|\mathbf{z}_k)$ can be represented as the following equation:

$$\begin{aligned} &p\big(\mathbf{x}_k|\mathbf{z}_k\big) \\ &= \frac{\Gamma\big(\tilde{\alpha} + \frac{n_{dx}}{2}\big)}{\Gamma(\tilde{\alpha})} \frac{1}{(2\tilde{\beta}\pi)^{\frac{n_{dx}}{2}}} \frac{1}{\sqrt{|\tilde{\mathbf{\Sigma}}|}} \left(1 + \frac{\Delta_x^2}{2\tilde{\beta}}\right)^{-\frac{n_{dx}}{2}-\tilde{\alpha}} \end{aligned} \tag{21}$$

where $\tilde{\alpha} = \alpha + (n_{dz}/2)$, $\tilde{\beta} = (1/2)(2\beta + \Delta_z^2)$, $\tilde{\mathbf{\Sigma}} = \mathbf{\Sigma}_{11} - \mathbf{\Sigma}_{12}\mathbf{\Sigma}_{22}^{-1}\mathbf{\Sigma}_{12}^T$, and $\Delta_x^2 = (\mathbf{x}_k - \hat{\mathbf{x}}_k^+)^T \tilde{\mathbf{\Sigma}}^{-1} (\mathbf{x}_k - \hat{\mathbf{x}}_k^+)$.

The derivation result (21) reveals that the conditional density of the state $p\left(\mathbf{x}_k|\mathbf{z}_k\right)$ is also a Student's t distribution, and parameterized in terms of $\tilde{\alpha}$ and $\tilde{\beta}$. Then, considering (15) and (17), and converting them back to the ν parameterization (7), we obtain

$$\begin{aligned} \eta_k &= 2\tilde{\alpha} = \eta_{k-1} + n_{dz} \\ \hat{\mathbf{x}}_k^+ &= \hat{\mathbf{x}}_k^- + \mathbf{\Sigma}_k^- \mathbf{H}_k^T \big(\mathbf{H}_k \mathbf{\Sigma}_k^- \mathbf{H}_k^T + \mathbf{R}_k\big)^{-1} \big(\mathbf{z}_k - \mathbf{h}\big(\hat{\mathbf{x}}_k^-, \mathbf{0}\big)\big) \\ \mathbf{\Sigma}_k^+ &= \frac{\tilde{\beta}}{\tilde{\alpha}} \tilde{\mathbf{\Sigma}} = \frac{\eta_{k-1} + \Delta_z^2}{\eta_{k-1} + n_{dz}} \\ &\quad \times \big(\mathbf{\Sigma}_k^- - \mathbf{\Sigma}_k^- \mathbf{H}_k^T \big(\mathbf{H}_k \mathbf{\Sigma}_k^- \mathbf{H}_k^T + \mathbf{R}_k\big)^{-1} \mathbf{H}_k \mathbf{\Sigma}_k^-\big) \\ \mathbf{P}_k^+ &= \frac{\eta_k}{\eta_k - 2} \mathbf{\Sigma}_k^+, \end{aligned} \tag{22}$$

where $\Delta_z^2 = (\mathbf{z}_k - \mathbf{h}(\hat{\mathbf{x}}_k^-, \mathbf{0}))^T (\mathbf{H}_k \mathbf{\Sigma}_k^- \mathbf{H}_k^T + \mathbf{R}_k)^{-1}$ $(\mathbf{z}_k - \mathbf{h}(\hat{\mathbf{x}}_k^-, \mathbf{0}))$.

The derivation result (22) can be summarized as follows.

Remark 2: Suppose that the random vectors $\mathbf{x}$ and $\mathbf{z}$ with dimensions n_{dx} and n_{dz}, respectively, are jointly distributed according to a multivariate Student's t distribution as

$$p(\mathbf{x}, \mathbf{z}) = \mathrm{St}\left(\begin{bmatrix}\mathbf{x} \\ \mathbf{z}\end{bmatrix}; \begin{bmatrix}\hat{\mathbf{x}} \\ \hat{\mathbf{z}}\end{bmatrix}, \begin{bmatrix}\mathbf{\Sigma}_{xx} & \mathbf{\Sigma}_{xz} \\ \mathbf{\Sigma}_{zx} & \mathbf{\Sigma}_{zz}\end{bmatrix}, \nu\right) \tag{23}$$

with $\nu > 2$. Then, the conditional density for $\mathbf{x}$ given the measurement $\mathbf{z}$ is also a Student's t distribution

$$p(\mathbf{x}|\mathbf{z}) = \mathrm{St}(\mathbf{x}; \boldsymbol{\mu}, \mathbf{\Sigma}, \nu + n_{dz}) \tag{24}$$

where

$$\begin{aligned} \boldsymbol{\mu} &= \hat{\mathbf{x}} + \mathbf{\Sigma}_{xz} \mathbf{\Sigma}_{zz}^{-1} (\mathbf{z} - \hat{\mathbf{z}}) \\ \Delta_z^2 &= (\mathbf{z} - \hat{\mathbf{z}})^T \mathbf{\Sigma}_{zz}^{-1} (\mathbf{z} - \hat{\mathbf{z}}) \\ \mathbf{\Sigma} &= \frac{\nu + \Delta_z^2}{\nu + n_{dz}} \big(\mathbf{\Sigma}_{xx} - \mathbf{\Sigma}_{xz} \mathbf{\Sigma}_{zz}^{-1} \mathbf{\Sigma}_{xz}^T\big). \end{aligned} \tag{25}$$

The details of the derivation of Remark 2 are presented in the Appendix.

B. Some Discussions About SEKF

An important assumption in Section III-A is that the prediction density is also a Student's t distribution and the DOF η_{k-1} is not changed by nonlinear transformation. Strictly speaking, the transformed density does not remain a standard Student's t distribution. However, the same problem exists in the EKF, and the prediction distribution is approximated as a Gaussian distribution after nonlinear transformation. Here, we adopt the same approximation strategy and this approximation is mild and commonly accepted [24].

According to the first equation of (22), it is not hard to establish that the DOF η_k increases with the filter recursion. However, the most important postulation in the SEKF algorithm is that the state and process/measurement noises are jointly Student's t distributed with a common DOF as shown in (13) and (16), namely, $\eta_{k-1} = \gamma = \delta$. To validate the assumption, it is clearly required that the noise DOF values γ and δ increase with the recursion process, which will lead to a conventional EKF after a few time steps. It can also be observed when letting the DOF $\eta_k \to \infty$, we can recover the Gaussian conditional covariance according to (22) as

$$\lim_{\eta_k \to \infty} \mathbf{\Sigma}_k^+ = \mathbf{\Sigma}_k^- - \mathbf{\Sigma}_k^- \mathbf{H}_k^T \big(\mathbf{H}_k \mathbf{\Sigma}_k^- \mathbf{H}_k^T + \mathbf{R}_k\big)^{-1} \mathbf{H}_k \mathbf{\Sigma}_k^-. \tag{26}$$

Thus, the growth of the DOF should be prevented and a heavy-tailed posterior density can thereby be retained throughout time. To bound the DOF, we first select a common DOF at time step $k-1$ for the jointly Student's t distribution of state $\hat{\mathbf{x}}_{k-1}^+$ and process noise $\mathbf{w}_{k-1}$ as

$$\eta'_{k-1} = \min(\eta_{k-1}, \gamma). \tag{27}$$

Generally, it follows that $\eta_{k-1} > \gamma$ (because $\eta_{k-1} = \eta_{k-2} + n_{dz}$) and then $\eta'_{k-1} = \gamma$. Consequently, the marginal density $p(\mathbf{x}_{k-1})$ should be adjusted given the new DOF η'_{k-1}. This problem is formulated as finding a scalar factor c such that the densities

$$\begin{aligned} p(\mathbf{x}_{k-1}) &= \mathrm{St}\big(\mathbf{x}_{k-1}; \hat{\mathbf{x}}_{k-1}^+, \mathbf{\Sigma}_{k-1}^+, \eta_{k-1}\big) \\ \tilde{p}(\mathbf{x}_{k-1}) &= \mathrm{St}\big(\mathbf{x}_{k-1}; \hat{\mathbf{x}}_{k-1}^+, c\mathbf{\Sigma}_{k-1}^+, \eta'_{k-1}\big) \end{aligned} \tag{28}$$

are similar in some sense to the specified one. This approximation step is important to the performance of a Student's t-based filter. To find the scalar factor c, we can use the moment matching (MM) method [43]. Considering (8), there is

$$\frac{\eta_{k-1}}{\eta_{k-1}-2}\mathbf{\Sigma}_{k-1}^{+}=\frac{\eta'_{k-1}}{\eta'_{k-1}-2}c\mathbf{\Sigma}_{k-1}^{+} \tag{29}$$

for $\eta_{k-1}>2$ and $\eta'_{k-1}>2$. The resulting scale factor c is then calculated as

$$c=\frac{\eta_{k-1}\left(\eta'_{k-1}-2\right)}{\left(\eta_{k-1}-2\right)\eta'_{k-1}}. \tag{30}$$

Then, the adjusted symmetric matrix $\tilde{\mathbf{\Sigma}}_{k-1}^{+}=c\mathbf{\Sigma}_{k-1}^{+}$ is used to update the predicted symmetric matrix as

$$\mathbf{\Sigma}_{k}^{-}=\mathbf{F}_{\mathbf{x}_{k-1}}\tilde{\mathbf{\Sigma}}_{k-1}^{+}\mathbf{F}_{\mathbf{x}_{k-1}}^{T}+\mathbf{F}_{\mathbf{w}_{k-1}}\mathbf{Q}_{k-1}\mathbf{F}_{\mathbf{w}_{k-1}}^{T}. \tag{31}$$

Similarly, this approximation step should be performed again before the measurement update step as

$$\begin{aligned}\eta''_{k-1}&=\min\left(\eta'_{k-1},\delta\right)\\ \text{if }\eta'_{k-1}>\delta&\begin{cases}d=\dfrac{\eta'_{k-1}(\delta-2)}{\left(\eta'_{k-1}-2\right)\delta}\\ \tilde{\mathbf{\Sigma}}_{k}^{-}=d\mathbf{\Sigma}_{k}^{-}\end{cases}\\ \text{if }\eta'_{k-1}<\delta&\begin{cases}e=\dfrac{\delta\left(\eta'_{k-1}-2\right)}{(\delta-2)\eta'_{k-1}}\\ \tilde{\mathbf{R}}_{k}=e\mathbf{R}_{k}\end{cases}\end{aligned} \tag{32}$$

where d and e are the scale factors, $\tilde{\mathbf{\Sigma}}_{k}^{-}$ and $\tilde{\mathbf{R}}_{k}$ are the predicted symmetric matrix of state and measurement noises, respectively, and δ is the DOF value of the measurement noise. Note that if $\eta'_{k-1}=\delta$, the approximation step (32) can be omitted.

In addition to the MM method, an alternative method to finding the scale factor is by minimization of the Kullback–Leibler divergence (KLD). KLD is a measure of how one probability distribution diverges from a second expected probability distribution, such as the observed distribution and the considered model. Taking the two densities as shown in (28) represented as $p(\mathbf{x})=\mathrm{St}(\mathbf{x};\mathbf{0},\mathbf{\Sigma},\nu)$ and $q(\mathbf{x})=\mathrm{St}(\mathbf{x};\mathbf{0},c\mathbf{\Sigma},\nu')$ as an example, the KLD is defined as [42]

$$\begin{aligned}D_{\mathrm{KL}}(p\parallel q)&=-\int\mathrm{St}(\mathbf{x};\mathbf{0},\mathbf{\Sigma},\nu)\ln\left(\frac{\mathrm{St}(\mathbf{x};\mathbf{0},c\mathbf{\Sigma},\nu')}{\mathrm{St}(\mathbf{x};\mathbf{0},\mathbf{\Sigma},\nu)}\right)d\mathbf{x}\\ &=-\int\mathrm{St}(\tilde{\mathbf{x}};\mathbf{0},\mathbf{I},\nu)\ln\left(\frac{\mathrm{St}(\tilde{\mathbf{x}};\mathbf{0},c\mathbf{I},\nu')}{\mathrm{St}(\tilde{\mathbf{x}};\mathbf{0},\mathbf{I},\nu)}\right)d\tilde{\mathbf{x}}\end{aligned} \tag{33}$$

where the stochastic decoupling technique is used to simplify the calculation of KLD. It is easy to find that the KLD is only related to the DOF values ν and ν' together with n_{dx}, without depending on the symmetric matrix $\mathbf{\Sigma}$. Furthermore, (33) can be written as

$$\begin{aligned}D_{\mathrm{KL}}(p\parallel q)&=-\int\mathrm{St}(\tilde{\mathbf{x}};\mathbf{0},\mathbf{I},\nu)\ln\left(\frac{\mathrm{St}(\tilde{\mathbf{x}};\mathbf{0},c\mathbf{I},\nu')}{\mathrm{St}(\tilde{\mathbf{x}};\mathbf{0},\mathbf{I},\nu)}\right)d\tilde{\mathbf{x}}\\ &=-\int\mathrm{St}(\tilde{\mathbf{x}};\mathbf{0},\mathbf{I},\nu)\ln(\mathrm{St}(\tilde{\mathbf{x}};\mathbf{0},c\mathbf{I},\nu'))d\tilde{\mathbf{x}}\\ &\quad+\int\mathrm{St}(\tilde{\mathbf{x}};\mathbf{0},\mathbf{I},\nu)\ln(\mathrm{St}(\tilde{\mathbf{x}};\mathbf{0},\mathbf{I},\nu))d\tilde{\mathbf{x}}.\end{aligned} \tag{34}$$

It can be seen that the second term of (34) is not related to the scale factor c, thereby we only need to minimize the first term of (34) to find the scale factor c. The objective function $J(c)$ can be written in the following equation:

$$J(c)=\min\left(-\int\mathrm{St}(\tilde{\mathbf{x}};\mathbf{0},\mathbf{I},\nu)\ln(\mathrm{St}(\tilde{\mathbf{x}};\mathbf{0},c\mathbf{I},\nu'))d\tilde{\mathbf{x}}\right). \tag{35}$$

Obviously, we can use the Monte Carlo integration method to solve this optimization problem offline. The results for scale facttor c with different DOF values when $n_{dx}=3$ and $n_{dx}=10$ are shown in Tables I and II.

TABLE I

OPTIMAL SCALAR FACTOR c WHEN $n_{dx}=3$

ν \ ν'	3	4	5	6	7
4	0.79(0.67)	1	NaN	NaN	NaN
5	0.58(0.56)	0.84(0.83)	1	NaN	NaN
6	0.46(0.50)	0.65(0.75)	0.85(0.90)	1	NaN
7	0.38(0.47)	0.54(0.70)	0.72(0.84)	0.87(0.93)	1
8	0.32(0.44)	0.45(0.67)	0.59(0.80)	0.74(0.89)	0.89(0.95)

TABLE II

OPTIMAL SCALAR FACTOR c WHEN $n_{dx}=10$

ν \ ν'	3	4	5	6	7
4	1(0.67)	1	NaN	NaN	NaN
5	0.73(0.56)	1(0.83)	1	NaN	NaN
6	0.58(0.50)	0.77(0.75)	0.99(0.85)	1	NaN
7	0.47(0.47)	0.64(0.7)	0.81(0.84)	0.97(0.93)	1
8	0.40(0.44)	0.53(0.67)	0.69(0.80)	0.83(0.89)	0.98(0.95)

Note that the result in the parentheses is the scalar factor c calculated by the MM method. It can be found that the scalar factor c calculated by the two approximation methods is different, and the MM method does not rely on the dimension n_{dx}. On the contrary, the scalar factor c calculated by the KLD method is related to the dimension n_{dx}, and the larger dimension n_{dx}, the smaller the difference in the calculated scalar factor c between the MM method and the KLD method. The performance of these two approximation methods will be discussed in Section V.

Considering the approximation step (take the MM approximation method as example), the complete Student's t extended Kalman filtering algorithm is summarized in Section IV.

IV. SIMULATION STUDIES

In this section, we present the simulation test results that demonstrate the validity of the robust CN algorithm for multiple AUVs based on the Student's t distribution.

Algorithm 1 SEKF Algorithm

Inputs: Initialize $\hat{\mathbf{x}}_0$, $\mathbf{\Sigma}_0$, $\mathbf{Q}_k$, $\mathbf{R}_k$, $\mathbf{z}_{1:T}$, η_0, γ, δ

For $k = 1{:}T$ Perform the following:

a. Perform the approximation of the common DOF and calculate the scale factor c using the MM method as (27), (30).

$$\eta'_{k-1} = \min(\eta_{k-1}, \gamma)$$
$$c = \frac{\eta_{k-1}(\eta'_{k-1} - 2)}{(\eta_{k-1} - 2)\eta'_{k-1}}.$$

b. Adjust the corresponding symmetric matrix.

$$\mathbf{\Sigma}^+_{k-1} \to c\mathbf{\Sigma}^+_{k-1}.$$

c. Compute the Jacobian matrices of process equation $\mathbf{F}_{\mathbf{x}_{k-1}}$, $\mathbf{F}_{\mathbf{w}_{k-1}}$, and perform the time update of the predicted state $\hat{\mathbf{x}}^-_k$ and symmetric matrix $\mathbf{\Sigma}^-_k$ as (15).

$$\hat{\mathbf{x}}^-_k = \mathbf{f}\left(\hat{\mathbf{x}}^+_{k-1}, \mathbf{u}_k, \mathbf{0}\right)$$
$$\mathbf{\Sigma}^-_k = \mathbf{F}_{\mathbf{x}_{k-1}}\mathbf{\Sigma}^+_{k-1}\mathbf{F}^T_{\mathbf{x}_{k-1}} + \mathbf{F}_{\mathbf{w}_{k-1}}\mathbf{Q}_{k-1}\mathbf{F}^T_{\mathbf{w}_{k-1}}.$$

d. Perform the approximation of the common DOF and corresponding adjustment of symmetric matrix for the predicted state $\hat{\mathbf{x}}^-_k$ and the measurement noise $\mathbf{R}_k$, if $\gamma \neq \delta$.

e. Compute the Jacobian matrix of measurement equation $\mathbf{H}_k$, and perform the measurement update of the estimated state $\hat{\mathbf{x}}^+_k$ and symmetric matrix $\mathbf{\Sigma}^+_k$ as (22).

$$\hat{\mathbf{x}}^+_k = \hat{\mathbf{x}}^-_k + \mathbf{\Sigma}^-_k\mathbf{H}^T_k\left(\mathbf{H}_k\mathbf{\Sigma}^-_k\mathbf{H}^T_k + \mathbf{R}_k\right)^{-1}\left(\mathbf{z}_k - \mathbf{h}\left(\hat{\mathbf{x}}^-_k, \mathbf{0}\right)\right), \mathbf{\Sigma}^+_k$$
$$= \frac{\eta_{k-1} + \Delta^2_z}{\eta_{k-1} + n_{dz}} \times\left(\mathbf{\Sigma}^-_k - \mathbf{\Sigma}^-_k\mathbf{H}^T_k\left(\mathbf{H}_k\mathbf{\Sigma}^-_k\mathbf{H}^T_k + \mathbf{R}_k\right)^{-1}\mathbf{H}_k\mathbf{\Sigma}^-_k\right).$$

f. Update the dof and calculate the estimation-error covariance.

$$\eta_{k-1} \to \eta_k$$
$$\mathbf{P}^+_k = \frac{\eta_k}{\eta_k - 2}\mathbf{\Sigma}^+_k.$$

Outputs: $\left\{\hat{\mathbf{x}}^+_k, \mathbf{\Sigma}^+_k \;\; 0 \leq k \leq T\right\}$

In the simulation test, the slave AUV received the accurate position of the leader AUV and the range measurement between the leader AUV and the slave AUV periodically. The conventional EKF is widely used in the field of CN because of its appropriate filtering accuracy and computational burden, and it has been verified fully in practical engineering. Therefore, the conventional EKF-based CN algorithm and the proposed SEKF-based CN algorithm are both used to estimate all the states of the slave AUV and their performances are compared in this section. In addition, the performance of EKF with threshold (threshold EKF, for short) is also given to validate the superiority of the proposed SEKF-based CN algorithm. In the threshold EKF, we employ the well-known Mahalanobis distance to gate the outliers, and this is a common and simple method to detect and reject outliers in actual projects [44]. On the receipt of a new measurement at time step k, the following expression is employed to compute the

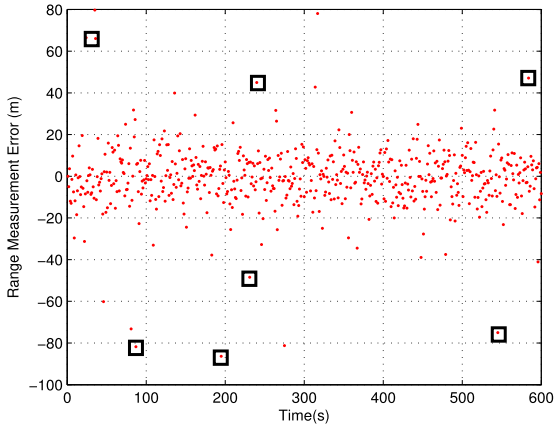

Fig. 3. Measurement noise of range between the leader AUV and the slave AUV, and the dots marked by black squares are some outliers.

Mahalanobis distance as:

$$\chi^2 = \left(\mathbf{z}_k - \mathbf{h}\left(\hat{\mathbf{x}}^-_k, \mathbf{0}\right)\right)^T\mathbf{S}^{-1}_k\left(\mathbf{z}_k - \mathbf{h}\left(\hat{\mathbf{x}}^-_k, \mathbf{0}\right)\right) \tag{36}$$

where $\mathbf{S}_k = \mathbf{H}_k\mathbf{P}^-_k\mathbf{H}^T_k + \mathbf{R}_k$.

A probabilistic threshold γ on this distance is used to specify whether the measurement can be used or not. A validated measurement is then used in the estimation step of the threshold EKF to correct the predicted states. On the contrary, a measurement that does not pass this test is regarded as an outlier, and the previous measurement at time step $k-1$ is retained to replace this outlier. Note that the control inputs $\hat{v}_k$, $\hat{\omega}_k$, and $\hat{\theta}_k$ are also pretreated by the threshold setting to detect and reject the outliers, and the same replacing strategy is also adopted.

To improve the observability of the CN system, the leader AUV sails in a zigzag maneuvering pattern [40]. The forward velocity v_k and the starboard velocity ω_k of the slave AUV are set as $v_k = \omega_k = 3$ m/s. The heading angle of the slave AUV changes as a sinusoid function

$$\theta_k = 1^\circ \cdot \sin(3 \cdot \pi \cdot k/\text{nlength}) \tag{37}$$

where the symbol k denotes the kth time step, and we consider $n$length $= 600$ time steps for each simulation test.

The process noise $\mathbf{w}_k$ and measurement noise $\mathbf{v}_k$ are both set to follow a Student's t distribution, and the outlier corrupted process noise and measurement noise that are uncorrelated white processes are generated according to the following equation:

$$\mathbf{w}_k \sim \begin{cases}\mathcal{N}(0, \mathbf{Q}) & \text{w.p. } 0.95\\ \mathcal{N}(0, 50\mathbf{Q}) & \text{w.p. } 0.05\end{cases} \tag{38}$$

$$\mathbf{v}_k \sim \begin{cases}\mathcal{N}(0, \mathbf{R}) & \text{w.p. } 0.90\\ \mathcal{N}(0, 5\mathbf{R}) & \text{w.p. } 0.10\end{cases} \tag{39}$$

where w.p. denotes "with probability." $\mathbf{Q}$ and $\mathbf{R}$ are nominal process noise and measurement noise covariance matrices, and they are set as $\mathbf{Q} = \text{diag}([0.5 \text{ m/s}, 0.5 \text{ m/s}, 1^\circ]^2)$ and $\mathbf{R} = \text{diag}([10 \text{ m}]^2)$. The process noise and measurement noise, which are generated according to (38) and (39), have heavy tails and approximatively follow a Student's t distribution.

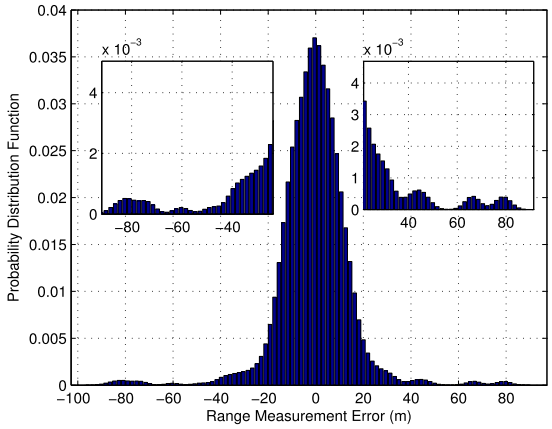

Fig. 4. PDF of the measurement noise, and the partial enlarged figures highlight the presence of the heavy tail of the noise distribution.

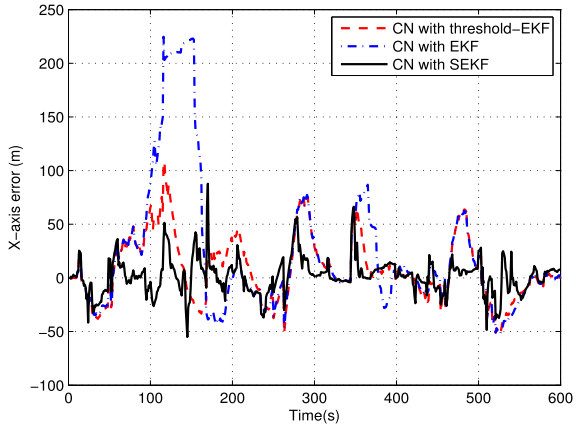

Fig. 5. Position estimation error along the x-axis with the conventional EKF-based CN algorithm (blue dashed and dotted line), the threshold EKF-based CN algorithm (red dashed line), and the proposed SEKF-based CN algorithm (black solid line).

For instance, the measurement noise (range between the leader AUV and the slave AUV) is drawn in Fig. 3, and its pdf is shown in Fig. 4. It can be seen that some outliers, which are marked by black squares, exist in the measurement noise which lead to the heavy-tailed distribution in Fig. 4.

In order to preserve as heavy tails as possible in the Student's t distribution, the DOF value for the SEKF-based CN algorithm is chosen as 3 [36]. The simulation tests were carried out in MATLAB on a computer with an Intel(R) Core(TM) i5-4300U CPU 1.90 GHz and 8 GB of RAM.

The position estimation errors along the x-axis and y-axis are drawn in Figs. 5 and 6. It is shown that the outliers existing in the process and measurement noises lead to a significant bias and a long period of time for reconvergence to the correct position estimate in the conventional EKF-based CN algorithm. In the threshold EKF, the bias induced by the outliers can be decreased. Although the influence of outliers can be eliminated by the threshold checking technology to some extent, the performance of the threshold EKF is not satisfactory. When outliers arise in the high maneuver, such as the zigzag maneuver, the replacement of an outlier with the previous measurement or control input, which usually changes

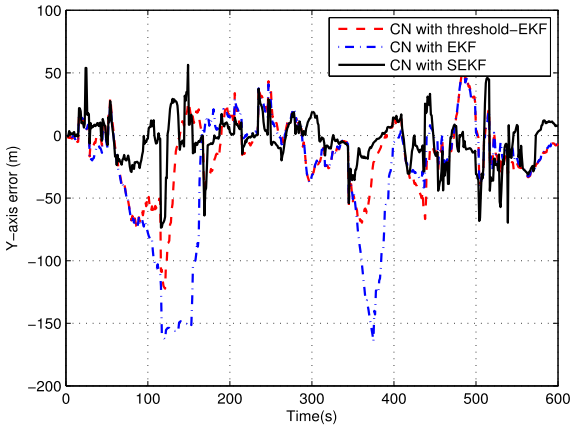

Fig. 6. Position estimation error along the y-axis with the conventional EKF-based CN algorithm (blue dashed and dotted line), the threshold EKF-based CN algorithm (red dashed line), and the proposed SEKF-based CN algorithm (black solid line).

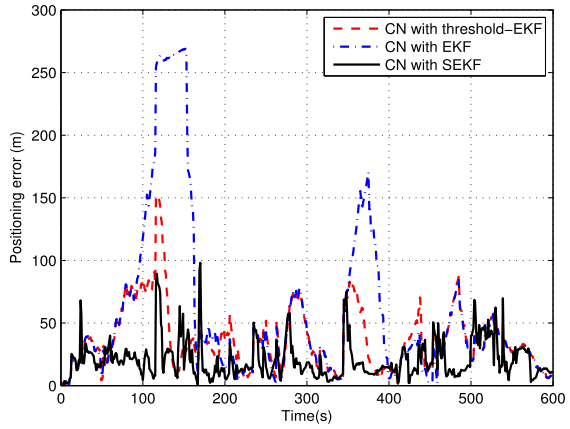

Fig. 7. Positioning error with the conventional EKF-based CN algorithm (blue dashed and dotted line), the threshold EKF-based CN algorithm (red dashed line), and the proposed SEKF-based CN algorithm (black solid line).

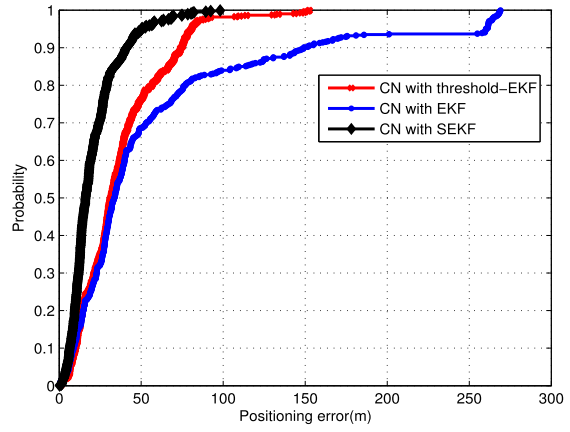

Fig. 8. CDF of positioning error.

rapidly between two time steps, will cause large positioning errors. In addition, an unreasonable manual threshold setting, which is usually not easy to choose without prior information, will also lead to a poor performance of the filter. Compared with the conventional EKF and the threshold EKF-based

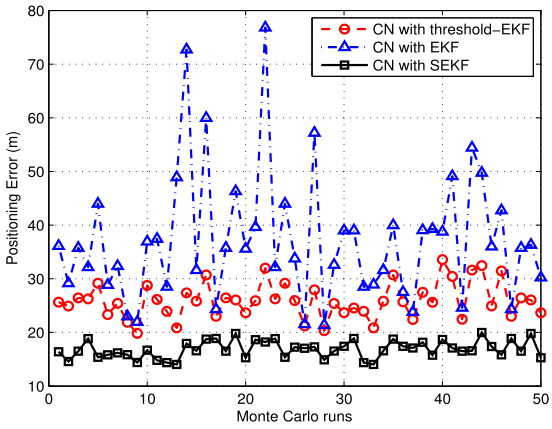

Fig. 9. Average positioning error with the conventional EKF-based CN algorithm (blue dashed and dotted line), the threshold EKF-based CN algorithm (red dashed line), and the proposed SEKF-based CN algorithm (black solid line) for 50 Monte Carlo runs.

CN algorithm, the SEKF-based CN algorithm can adjust quickly after a peak in the position estimation error.

In addition, the positioning error and its cumulative distribution function (CDF) of the slave AUV are drawn in Figs. 7 and 8. The average positioning error of the slave AUV is 57.87 m using the conventional EKF-based CN algorithm. Estimated by the threshold EKF, the performance of position estimation is improved with respect to the conventional EKF-based CN algorithm, and the average positioning error of the slave AUV is reduced to be 36.81 m. Correspondingly, the positioning accuracy is improved by 36.4%. Using the SEKF-based CN algorithm, the average positioning error is reduced to be 20.65 m, and the positioning accuracy is, respectively, improved by 64.32% and 43.91% with respect to the conventional EKF and threshold EKF-based CN algorithm. It can be found that the proposed SEKF-based CN algorithm outperformed the conventional EKF and threshold EKF-based CN algorithm in terms of the positioning error when outliers exist in the process noise and measurement noise.

Furthermore, the performance of the conventional EKF and the threshold EKF-based CN algorithm together with the proposed SEKF-based CN algorithm are compared in terms of execution time. A total of 50 Monte Carlo runs are performed, and the positioning error of the slave AUV is drawn in Fig. 9 for 50 Monte Carlo runs. In addition, the corresponding average positioning error and the average execution time are shown in Table III. It can be seen that the execution time of the conventional EKF and the threshold EKF-based CN algorithm is nearly the same, and the proposed SEKF-based CN algorithm is a little longer than that of the conventional EKF-based CN algorithm. This phenomenon is reasonable because of the additional step of approximation of common DOF parameters and the adjustment of a symmetric matrix, but such an increase in execution time can be considered negligible for many real-time applications.

V. Field Trial Results

To evaluate the performance of the proposed SEKF-based CN algorithm, the proposed scheme is applied by postprocessing the off-line data collected in a field trial.

TABLE III

AVERAGE POSITIONING ERROR AND THE AVERAGE EXECUTION TIME FOR 50 MONTE CARLO RUNS

CN algorithms	Positioning error	Execution time
EKF based CN algorithm	37.19 m	$0.095\,s$
threshold-EKF based CN algorithm	25.93 m	$0.096\,s$
SEKF based CN algorithm	17.86 m	$0.110\,s$

TABLE IV

PERFORMANCE PARAMETERS OF SENSORS

Sensors	Metric	Parameters
Magnetic Compass	Random noise	$1\ deg$
DVL	Working range	$-150\,m/s \sim 200\,m/s$
	Measurement accuracy	$0.1\,\%$

The field trial was conducted in October 2014 in Lake Thai where the average depth is about 6.5 ft. Due to the limitations of the field trial conditions, we used two survey vessels to replace the AUVs. In the field trial, one survey vessel (denoted as vessel A) acted as the leader AUV and another survey vessel (denoted as vessel B) is the slaver AUV. Two survey vessels are both equipped with an underwater acoustic modem S2CR 7/17 produced by Evologics, and thereby anyone of them can broadcast information to another through the two-way acoustic communication technique.

On the vessel A, a GPS is equipped to provide accurate positioning information. Through the acoustic communication equipment, acoustic data packets including the range measurement and accurate position of vessel A are transmitted to the vessel B every 10 s. On the vessel B, a magnetic compass is equipped to measure the heading angle of the vessel B, and a DVL that works in the mode of bottom track is used to supply the velocity of the vessel B. The data collected by the magnetic compass and the DVL are used to calculate a DR navigation solution for the vessel B. The performance parameters of the magnetic compass and the DVL are listed in Table IV. In addition, a PHINS produced by iXBlue works in the integrated mode and it is also equipped on the vessel B to provide the benchmark for position, velocity, and attitude.

The trajectories of the vessel A and the vessel B together with the DR solution of vessel B are drawn in Fig. 10. It can be seen that the DR solution of the vessel B (blue solid line) gradually diverges from the true trajectory (red dashed line) because of the accumulated positioning error from the DR solution. In addition, the velocity of the vessel B is projected on the navigation reference frame by the heading angle from the magnetic compass and they are drawn in Fig. 11 (top). To evaluate the robustness of the proposed SEKF-based CN algorithm against outliers existing in the process noise, some outliers are added artificially in the velocity control input collected by the DVL as shown in Fig. 11 (top). Similarly, we add some large outliers in the range measurement from underwater acoustic communication system to simulate the stringent conditions existing in the shallow water with low-quality acoustic communication equipments, thereby we can see some outliers in the range measurement noise in Fig. 11 (bottom).

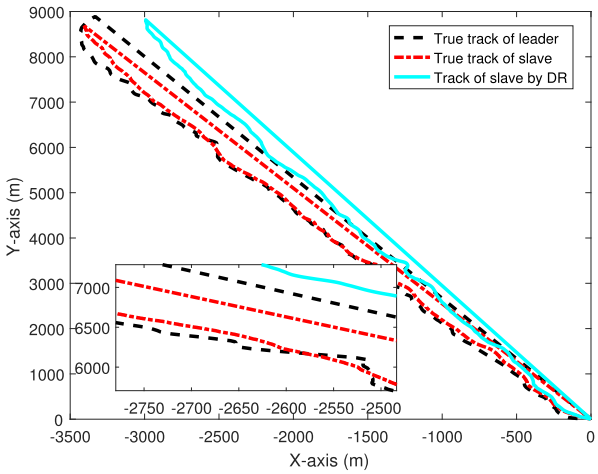

Fig. 10. Paths taken by the vessel A and the vessel B during the field trial, together with the DR solution of the vessel B.

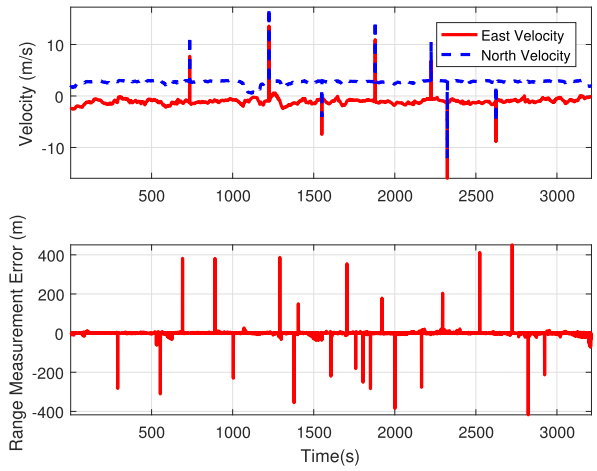

Fig. 11. Velocity of vessel B and measurement noise of range between vessel A and vessel B with some artificial outliers. The fore-and-aft velocity of vessel B is projected on the navigation reference frame by the heading angle.

TABLE V
AVERAGE POSITIONING ERROR WITH DIFFERENT DOF VALUES IN THE SEKF-BASED CN ALGORITHM

dof	ν=3	ν=4	ν=5	ν=6	ν=7 (optimal)
RMSE	32.01	20.42	17.37	16.31	16.09
dof	ν =8	ν =9	ν =10	ν =11	ν =12
RMSE	16.42	17.13	18.52	21.08	22.89

The field trial results are shown in Table V and Figs. 12–14. In the field trial, the performance of the conventional EKF, the threshold EKF, and the SEKF-based CN algorithm is compared. The threshold is set as $\gamma = 15$ in the threshold EKF-based CN algorithm. In the SEKF-based CN algorithm, the MM approximation method is adopted to find the scalar factor c. In addition, the DOF value that determines the tail behavior of the Student's t distribution in the SEKF-based CN algorithm is related to the properties of the outliers, and the performance of the Student's t-based filter is inconsistent as the DOF varies. However, the outliers are usually time-varying and unpredictable in practical engineering, and it is

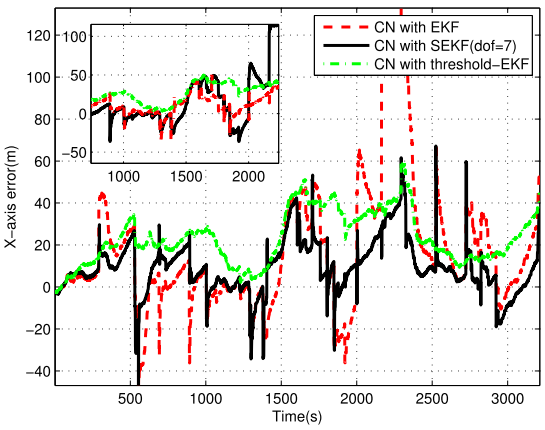

Fig. 12. x-axis position estimation error of three different CN algorithms. The threshold of threshold EKF is $\gamma = 15$ and the DOF value of SEKF is $\nu = 7$.

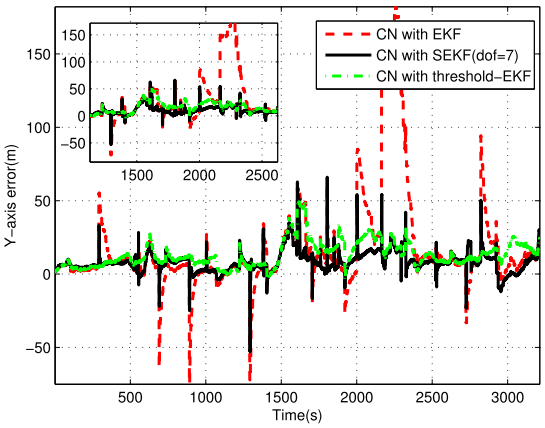

Fig. 13. y-axis position estimation error of three different CN algorithms. The threshold of threshold EKF is $\gamma = 15$ and the DOF value of SEKF is $\nu = 7$.

hard to determine a fixed DOF in advance. Therefore, we use the SEKF-based CN algorithm with different DOF values ($\nu = 3, 4, \ldots, 12$) to postprocess the data collected in the field trial, and the average positioning error is regarded as the measure of performance, as shown in Table V. The average positioning error is defined in the following equation:

$$\text{RMSE} = \frac{1}{T}\Sigma_{k=1}^{T}\sqrt{(x_k - \hat{x}_k)^2 + (y_k - \hat{y}_k)^2} \tag{40}$$

where (x_k, y_k) and $(\hat{x}_k, \hat{y}_k)$ are the true position and estimated position, respectively, at time step k, and T is the time length.

From Table V, it can be seen that the optimal DOF value is $\nu = 7$ in terms of the average positioning error. On the contrary, the DOF value $\nu = 3$, which is usually recommended in most works [35], [36], performs poorly here. Therefore, it is very important to choose an appropriate DOF value for the Student's t-based CN algorithm in practical engineering. Note that if not specified the DOF value of SEKF-based CN algorithm is chosen as $\nu = 7$ in the following.

The x-axis and y-axis position estimation errors of the conventional EKF, the threshold EKF, and the SEKF-based CN algorithm are shown in Figs. 12 and 13. It is shown that the outliers existing in the process and measurement noises have a significant negative effect on the performance

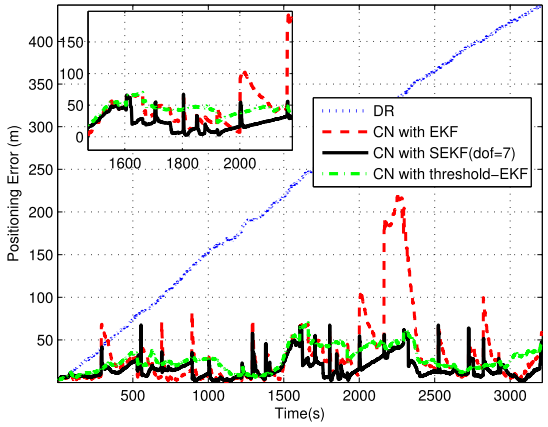

Fig. 14. DR solution and the positioning error of the conventional EKF, the threshold EKF, and the SEKF-based CN algorithm.

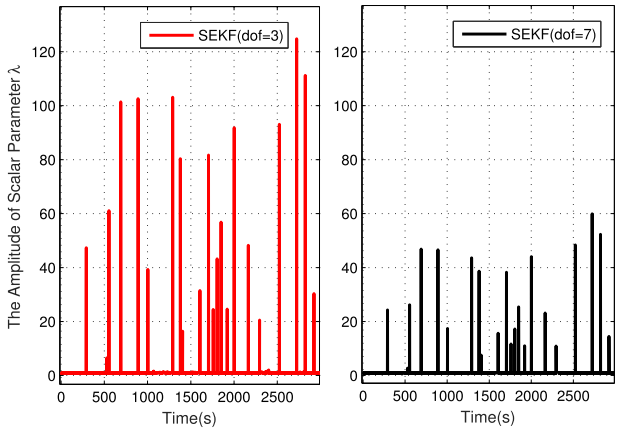

Fig. 15. Scalar parameter λ with different DOF values $\nu = 3$ and $\nu = 7$.

of the conventional EKF-based CN algorithm, leading to a significant bias and a long period of time for reconvergence to the correct position estimate. Especially, upon receipt of the outliers between the 2000 and 2200 s, the position estimation error jumps highly for the conventional EKF-based CN algorithm. In the threshold EKF-based CN algorithm, the influence of the outliers can be decreased, and the performance of threshold EKF even outperformed the SEKF on the receipt of several certain outliers. However, due to the approximation error induced by replacing strategy and the threshold setting error, the overall performance of the threshold EKF-based CN algorithm is worse than that of the SEKF-based CN algorithm. It can be seen that the SEKF-based CN algorithm can minimize the negative effect induced by all outliers existing in the control input and measurement, and it adjusts quickly after a peak in the position estimation error. Therefore, the proposed SEKF-based CN algorithm shows a better robustness against outliers existing in process and measurement noises, compared with the conventional EKF and the threshold EKF-based CN algorithm with a Gaussian distributed noise assumption.

Furthermore, Fig. 14 shows the positioning error of the DR solution, the conventional EKF and the threshold EKF-based CN algorithms together with the SEKF-based CN algorithm. The positioning error is defined in the following equation:

$$\text{Positioning Error}(k) = \sqrt{(x_k - \hat{x}_k)^2 + (y_k - \hat{y}_k)^2} \tag{41}$$

where (x_k, y_k) and $(\hat{x}_k, \hat{y}_k)$ are the true position and estimated position, respectively, at time step k.

It can be seen that the DR solution is unbounded with time, and the maximum positioning error is 433 m. In the CN scheme, the positioning error can be bounded effectively. The average positioning errors of the conventional EKF-based CN algorithm is 32.46 m. Estimated by the threshold EKF, the average positioning error is reduced to be 26.43 m, and the positioning accuracy is improved by 18.57%. Using the SEKF-based CN algorithm, the average positioning error is further reduced to be 16.09 m, and the positioning accuracy is correspondingly improved by 50.43%.

In addition, the average positioning error of SEKF-based CN algorithm ($\nu = 3$) is 32.01 m as shown in Table V, and the positioning accuracy is not improved much with respect to the conventional EKF-based CN algorithm. The main reason is that the DOF value $\nu = 3$ is inappropriate in terms of the added outliers. Although the DOF value $\nu = 3$ can cope with the extreme level heavy tailed distributed noise, the actual tail behavior of the Student's t distributed noise in practical engineering maybe at the intermediate level. In addition, we can conclude that the SEKF-based CN algorithm is close to the conventional EKF-based CN algorithm from the table of the SEKF algorithm, and the only time when it makes a difference is when the residual is large, and the estimation-error covariance $\mathbf{P}_k^+$ will be scaled in the following equation:

$$\mathbf{P}_k^+ = \frac{\eta_k}{\eta_k - 2} \cdot \tilde{\mathbf{\Sigma}}_k^+ = \frac{\eta_k}{\eta_k - 2} \cdot \lambda_k \cdot \mathbf{\Sigma}_k^+ \tag{42}$$

where $\tilde{\mathbf{\Sigma}}_k^+$ is the symmetric matrix of SEKF and $\mathbf{\Sigma}_k^+ = \mathbf{\Sigma}_k^- - \mathbf{\Sigma}_k^- \mathbf{H}_k^T (\mathbf{H}_k \mathbf{\Sigma}_k^- \mathbf{H}_k^T + \mathbf{R}_k)^{-1} \mathbf{H}_k \mathbf{\Sigma}_k^-$ which is the same as the estimation-error covariance in the conventional EKF. In addition, $\lambda_k = (\eta_{k-1} + \Delta_z^2/\eta_{k-1} + n_{dz})$ can be seen as a scale parameter which will enlarge the estimation-error covariance $\mathbf{P}_k^+$ when outliers occur. With different DOF values ($\nu = 3, 7$), the value of scale parameter λ_k is shown in Fig. 15. It can be seen that the scalar parameter λ will become larger when outlier appears. In addition, the smaller the DOF value ν, the larger will be the scale parameter λ. If the scale parameter λ is too large, the estimation-error covariance $\mathbf{P}_k^+$ will be greatly enlarged, which will degrade the performance of the SEKF-based CN algorithm. On the contrary, if the selected DOF value is appropriate ($\nu = 7$), the estimation-error covariance $\mathbf{P}_k^+$ will be suitably enlarged to minimize the negative effect induced by the outliers. This is the main reason that the Student's t distribution-based filter shows an improved robustness against outliers by adjusting the DOF ν, compared with the Gaussian distribution-based filters. In conclusion, an appropriate DOF is the guarantee of the performance of SEKF-based CN algorithm. An effective way to select an appropriate DOF for Student's t distribution is to evaluate the noise characteristics with prior information in advance. If the noise is distributed by an extreme level heavy-tailed distribution, the SEKF-based CN algorithm with $\nu = 3$ can cope with the outliers well. Instead of an extreme level heavy-tailed distributed noise, the filter with $3 < \nu < 15$ can cope with the intermediate level heavy tailed distributed

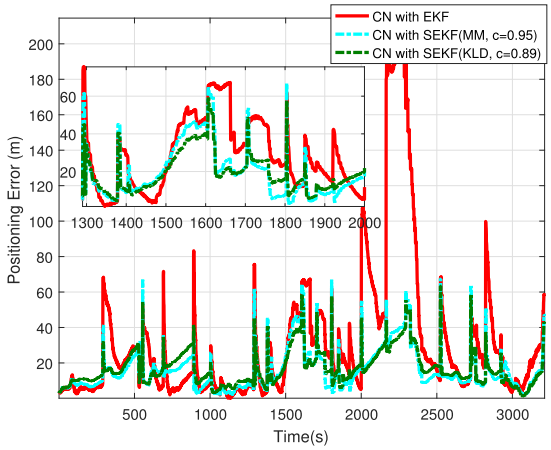

Fig. 16. Comparison of KLD approximation method and MM approximation method in terms of positioning error. The scale factor calculated by the KLD approximation method is $c = 0.89$ and the scale factor calculated by the MM approximation method is $c = 0.95$.

noise [45]. Furthermore, to cope with different kinds of outliers, an ensemble of SEKFs using different DOF values can be used, and we can select either a single "best" SEKF as the outlier varies, or combine the output from all SEKFs in a single solution.

In addition, the performances of the different approximation methods, namely, the KLD approximation method and MM approximation method discussed in Section III-B are compared in Fig. 16. The corresponding scale factors in terms of different approximation methods can be found in Table I. When the outlier appears, it can be seen that the peak of the positioning error based on the MM approximation method (scale factor $c = 0.95$) is higher than that of the positioning error based on the KLD approximation method (scale factor $c = 0.89$). Therefore, the KLD approximation method is better than the MM approximation method in terms of the stability and smoothness. However, the average positioning error of the KLD approximation-based CN algorithm is 17.02 m, so the performance of the MM approximation method is better than that of the KLD approximation method in terms of average positioning error. Therefore, it is reasonable to choose an appropriate approximation method in practical engineering according to specific requirements.

VI. Conclusion

In this paper, a robust Student's t extended Kalman filtering algorithm for a leader–slave CN system for AUVs is proposed. The heavy-tailed process and measurement noises induced by outliers from cheap but low-accuracy DR sensors and underwater acoustic communication system are modeled by a Student's t distribution, and the Student's t EKF for the nonlinear system was derived to estimate the states of the slave AUV with range information between slave AUV and leader AUV, which bounds the accumulated positioning error of the CN system. Two approximation methods, namely, the MM method and KLD method, which are required in the Student's t-based filter are discussed, and an optimal scalar factor calculated by these two approximation methods is given. The resulting algorithm was compared with a conventional EKF-based CN algorithm in a simulation evaluation. It was found that the proposed SEKF-based CN algorithm outperformed the conventional EKF-based CN algorithm in terms of positioning error when the process and measurement noise had heavy-tailed behavior. In the field trial, the performance of different DOF values is compared, and an optimal DOF value was chosen in terms of the positioning error. A link between the DOF value and the robust effect of the Student's t distribution is revealed. In addition, it is worth noting that this robust Student's t filter-based CN algorithm can be used either in a centralized or decentralized manner.

As mentioned in the field trial, the DOF value $\nu = 3$, which is usually recommended in most works, is not always optimal in practical engineering. An appropriate DOF should be selected according to the actual properties of the outliers. Thus, in the future work, we will study more about the relationship between the performance of the Student's t-based filter and the DOF, and investigate robust Student's t-based filters with a DOF automatically selected by itself.

Appendix

To calculate the conditional pdf $p(\mathbf{x}|\mathbf{z})$, we use the α, β parameterized form of joint pdf $p(\mathbf{x}, \mathbf{z})$ and marginal pdf $p(\mathbf{z})$ as

$$\begin{aligned} p(\mathbf{x}|\mathbf{z}) = \frac{p(\mathbf{x},\mathbf{z})}{p(\mathbf{z})} &= \frac{\Gamma\left(\alpha+\frac{n}{2}\right)}{\Gamma(\alpha)}\frac{1}{(2\beta\pi)^{\frac{n}{2}}} \\ &\times \frac{1}{\sqrt{|\tilde{\mathbf{\Sigma}}|}}\left(1+\frac{\Delta^2}{2\beta}\right)^{-\frac{n}{2}-\alpha} \\ &\times \left(\frac{\Gamma\left(\alpha+\frac{n_{dz}}{2}\right)}{\Gamma(\alpha)}\frac{1}{(2\beta\pi)^{\frac{n_{dz}}{2}}}\frac{1}{\sqrt{|\mathbf{\Sigma}_{zz}|}}\right. \\ &\left.\times\left(1+\frac{\Delta_z^2}{2\beta}\right)^{-\frac{n_{dz}}{2}-\alpha}\right)^{-1} \end{aligned} \tag{43}$$

where $\mathbf{x}$ is an n_{dx}-vector, $\mathbf{z}$ is an n_{dz}-vector, and $n = n_{dx} + n_{dz}$. $\tilde{\mathbf{\Sigma}}$ is the symmetric matrix of the joint density $p(\mathbf{x}, \mathbf{z})$, $\mathbf{\Sigma}_{zz}$ is the symmetric matrix of the marginal pdf $p(\mathbf{z})$, and $\alpha = \beta = (\nu/2)$. In addition, the quadratic form Δ_z^2 is defined in the following equation:

$$\Delta_z^2 = (\mathbf{z}-\hat{\mathbf{z}})^T\mathbf{\Sigma}_{zz}^{-1}(\mathbf{z}-\hat{\mathbf{z}}). \tag{44}$$

Then, the fourth term in (43) is rewritten as

$$\begin{aligned} \left(1+\frac{\Delta^2}{2\beta}\right)^{-\frac{n}{2}-\alpha} &= \left(1+\frac{\Delta_z^2}{2\beta}+\frac{\Delta_x^2}{2\beta}\right)^{-\frac{n}{2}-\alpha} \\ &= \left(1+\frac{\Delta_z^2}{2\beta}\right)^{-\frac{n}{2}-\alpha}\left(1+\frac{\Delta_x^2}{2\beta+\Delta_z^2}\right)^{-\frac{n}{2}-\alpha}. \end{aligned} \tag{45}$$

In (45), Δ_x^2 is introduced to turn (43) into the form of a Student's t distribution. The quantity Δ_x^2 is defined in (46), and $\Delta^2 = \Delta_x^2 + \Delta_z^2$, the derivation of which is straightforward and omitted [46], and given as

$$\Delta_x^2 = (\mathbf{x}-\boldsymbol{\mu})^T\left(\mathbf{\Sigma}_{xx}-\mathbf{\Sigma}_{xz}\mathbf{\Sigma}_{zz}^{-1}\mathbf{\Sigma}_{xz}^T\right)^{-1}(\mathbf{x}-\boldsymbol{\mu}) \tag{46}$$

where $\boldsymbol{\mu} = \hat{\mathbf{x}} + \boldsymbol{\Sigma}_{xz}\boldsymbol{\Sigma}_{zz}^{-1}\left(\mathbf{z} - \hat{\mathbf{z}}\right)$ and $\boldsymbol{\Sigma}_{ij}\,(i, j = x, z)$ is the corresponding element of the block matrix $\tilde{\boldsymbol{\Sigma}}$.

Considering (45), the exponential terms in (43) can be rewritten as

$$\left(1+\frac{\Delta_z^2}{2\beta}\right)^{-\frac{n}{2}-\alpha}\left(1+\frac{\Delta_x^2}{2\beta+\Delta_z^2}\right)^{-\frac{n}{2}-\alpha}\left(1+\frac{\Delta_z^2}{2\beta}\right)^{\frac{n_{dz}}{2}+\alpha} = \left(1+\frac{\Delta_z^2}{2\beta}\right)^{-\frac{n_{dx}}{2}}\left(1+\frac{\Delta_x^2}{2\beta+\Delta_z^2}\right)^{-\frac{n}{2}-\alpha}. \quad (47)$$

The remaining terms of (43) can be written as

$$\frac{\Gamma\left(\alpha+\frac{n}{2}\right)}{\Gamma\left(\alpha+\frac{n_{dz}}{2}\right)}\frac{(2\beta\pi)^{\frac{n_{dz}}{2}}}{(2\beta\pi)^{\frac{n}{2}}}\frac{\sqrt{|\boldsymbol{\Sigma}_{zz}|}}{\sqrt{|\tilde{\boldsymbol{\Sigma}}|}} = \frac{\Gamma\left(\alpha+\frac{n_{dz}}{2}+\frac{n_{dx}}{2}\right)}{\Gamma\left(\alpha+\frac{n_{dz}}{2}\right)}\frac{1}{(2\beta\pi)^{\frac{n_{dx}}{2}}}\sqrt{|\left(\boldsymbol{\Sigma}_{xx}-\boldsymbol{\Sigma}_{xz}\boldsymbol{\Sigma}_{zz}^{-1}\boldsymbol{\Sigma}_{xz}^{T}\right)^{-1}|}. \quad (48)$$

Combining (47) and (48) gives the transformation of (43)

$$\begin{aligned} p(\mathbf{x}|\mathbf{z}) &= \frac{\Gamma\left(\alpha+\frac{n_{dz}}{2}+\frac{n_{dx}}{2}\right)}{\Gamma\left(\alpha+\frac{n_{dz}}{2}\right)}\left(1+\frac{\Delta_x^2}{2\beta+\Delta_z^2}\right)^{-\frac{n}{2}-\alpha} \\ &\quad\times\frac{\sqrt{|\left(\boldsymbol{\Sigma}_{xx}-\boldsymbol{\Sigma}_{xz}\boldsymbol{\Sigma}_{zz}^{-1}\boldsymbol{\Sigma}_{xz}^{T}\right)^{-1}|}}{(2\beta\pi)^{\frac{n_{dx}}{2}}}\left(1+\frac{\Delta_z^2}{2\beta}\right)^{-\frac{n_{dx}}{2}} \\ &= \frac{\Gamma\left(\tilde{\alpha}+\frac{n_{dx}}{2}\right)}{\Gamma\left(\tilde{\alpha}\right)}\frac{1}{\left(2\tilde{\beta}\pi\right)^{\frac{n_{dx}}{2}}}\frac{1}{\sqrt{|\hat{\boldsymbol{\Sigma}}|}}\left(1+\frac{\Delta_x^2}{2\tilde{\beta}}\right)^{-\frac{n_{dx}}{2}-\tilde{\alpha}} \end{aligned} \quad (49)$$

where $\tilde{\alpha} = \alpha + (n_{dz}/2)$, $\tilde{\beta} = (1/2)(2\beta + \Delta_z^2)$, and $\hat{\boldsymbol{\Sigma}} = \boldsymbol{\Sigma}_{xx} - \boldsymbol{\Sigma}_{xz}\boldsymbol{\Sigma}_{zz}^{-1}\boldsymbol{\Sigma}_{xz}^{T}$.

It is clear that the conditional pdf $p(\mathbf{x}|\mathbf{z})$ also admits a Student's t distribution according to (49). Moreover, there is

$$\begin{aligned} \nu &= 2\tilde{\alpha} = \nu + n_{dz} \\ \boldsymbol{\mu} &= \hat{\mathbf{x}} + \boldsymbol{\Sigma}_{xz}\boldsymbol{\Sigma}_{zz}^{-1}(\mathbf{z} - \hat{\mathbf{z}}) \\ \boldsymbol{\Sigma} &= \frac{\tilde{\beta}}{\tilde{\alpha}}\hat{\boldsymbol{\Sigma}} = \frac{\nu+\Delta_z^2}{\nu+n_{dz}}\left(\boldsymbol{\Sigma}_{xx} - \boldsymbol{\Sigma}_{xz}\boldsymbol{\Sigma}_{zz}^{-1}\boldsymbol{\Sigma}_{xz}^{T}\right). \end{aligned} \quad (50)$$

REFERENCES

[1] L. Paull, S. Saeedi, M. Seto, and H. Li, "AUV navigation and localization: A review," *IEEE J. Ocean. Eng.*, vol. 39, no. 1, pp. 131–149, Jan. 2014.

[2] A. Bahr, J. J. Leonard, and M. F. Fallon, "Cooperative localization for autonomous underwater vehicles," *Int. J. Robot. Res.*, vol. 28, no. 6, pp. 714–728, 2009.

[3] J. Xu, H. He, F. Qin, and L. Chang, "A novel autonomous initial alignment method for strapdown inertial navigation system," *IEEE Trans. Instrum. Meas.*, vol. 69, no. 9, pp. 2274–2282, Sep. 2017.

[4] Z. J. Harris and L. L. Whitcomb, "Preliminary study of cooperative navigation of underwater vehicles without a DVL utilizing range and range-rate observations," in *Proc. IEEE Int. Conf. Robot. Autom. (ICRA)*, May 2016, pp. 2618–2624.

[5] E. Fiorelli, N. E. Leonard, P. Bhatta, D. A. Paley, R. Bachmayer, and D. M. Fratantoni, "Multi-AUV control and adaptive sampling in Monterey bay," *IEEE J. Ocean. Eng.*, vol. 31, no. 4, pp. 935–948, Oct. 2006.

[6] A. I. Mourikis and S. I. Roumeliotis, "Performance analysis of multirobot Cooperative localization," *IEEE Trans. Robot.*, vol. 22, no. 4, pp. 666–681, Aug. 2006.

[7] R. Sharma, R. Beard, C. Taylor, and S. Quebe, "Graph-based observability analysis of bearing-only cooperative localization," *IEEE Trans. Robot.*, vol. 28, no. 2, pp. 522–529, Apr. 2012.

[8] R. G. Lins, S. N. Givigi, and P. G. Kurka, "Vision-based measurement for localization of objects in 3-D for robotic applications," *IEEE Trans. Instrum. Meas.*, vol. 64, no. 11, pp. 2950–2958, Nov. 2015.

[9] G. Xiao, B. Wang, Z. Deng, M. Fu, and Y. Ling, "An acoustic communication time delays compensation approach for master–slave AUV cooperative navigation," *IEEE Sensors J.*, vol. 17, no. 2, pp. 504–513, Jan. 2016.

[10] A. R. Vetrella, G. Fasano, A. Renga, and D. Accardo, "Cooperative UAV navigation based on distributed multi-antenna GNSS, vision, and MEMS sensors," in *Proc. IEEE Int. Conf. Unmanned Aircraft Syst. (ICUAS)*, Jun. 2015, pp. 1128–1137.

[11] N. Alam, A. Kealy, and A. G. Dempster, "Cooperative inertial navigation for GNSS-challenged vehicular environments," *IEEE Trans. Intell. Transp. Syst.*, vol. 14, no. 3, pp. 1370–1379, Sep. 2013.

[12] N. Alam and A. G. Dempster, "Cooperative positioning for vehicular networks: Facts and future," *IEEE Trans. Intell. Transp. Syst.*, vol. 14, no. 4, pp. 1708–1717, Dec. 2013.

[13] H. Hlavacs and K. A. Hummel, "Cooperative positioning when using local position information: Theoretical framework and error analysis," *IEEE Trans. Mobile Comput.*, vol. 12, no. 10, pp. 2091–2104, Oct. 2013.

[14] S. I. Roumeliotis and G. A. Bekey, "Distributed multirobot localization," *IEEE Trans. Robot. Autom.*, vol. 18, no. 5, pp. 781–795, Oct. 2002.

[15] A. C. Sanderson, "A distributed algorithm for cooperative navigation among multiple mobile robots," *Adv. Robot.*, vol. 12, no. 4, pp. 335–349, 1997.

[16] A. Howard, M. J. Matark, and G. S. Sukhatme, "Localization for mobile robot teams using maximum likelihood estimation," in *Proc. IEEE/RSJ Int. Conf. Intell. Robots Syst.*, Sep./Oct. 2002, pp. 434–439.

[17] D. Fox, W. Burgard, H. Kruppa, and S. Thrun, "A probabilistic approach to collaborative multi-robot localization," *Auto. Robots*, vol. 8, no. 3, pp. 325–344, 2000.

[18] E. D. Nerurkar, S. I. Roumeliotis, and A. Martinelli, "Distributed maximum *a posteriori* estimation for multi-robot cooperative localization," in *Proc. IEEE Int. Conf. Robot. Autom.*, May 2009, pp. 1402–1409.

[19] I. M. Rekleitis, G. Dudek, and E. E. Milios, "Multi-robot cooperative localization: A study of trade-offs between efficiency and accuracy," in *Proc. IEEE/RSJ Int. Conf. Intell. Robots Syst.*, Sep./Oct. 2002, pp. 2690–2695.

[20] S. E. Webster, L. L. Whitcomb, and R. M. Eustice, "Advances in decentralized single-beacon acoustic navigation for underwater vehicles: Theory and simulation," in *Proc. IEEE/OES Auto. Underwater Vehicles*, Sep. 2010, pp. 1–8.

[21] S. Wang, L. Chen, D. Gu, and H. Hu, "Cooperative localization of AUVs using moving horizon estimation," *IEEE/CAA J. Autom. Sinica*, vol. 1, no. 1, pp. 68–76, Jan. 2014.

[22] W. Gao, J. Yang, J. Liu, H. Shi, and B. Xu, "Moving horizon estimation for cooperative localisation with communication delay," *J. Navigat.*, vol. 68, no. 3, pp. 493–510, 2015.

[23] E. Olson, J. J. Leonard, and S. Teller, "Robust range-only beacon localization," *IEEE J. Ocean. Eng.*, vol. 31, no. 4, pp. 949–958, Oct. 2006.

[24] F. Tronarp, R. Hostettler, and S. Särkkä, "Sigma-point filtering for nonlinear systems with non-additive heavy-tailed noise," in *Proc. Int. Conf. Inf. Fusion (FUSION)*, Jul. 2016, pp. 1859–1866.

[25] J. Vaganay, J. J. Leonard, and J. G. Bellingham, "Outlier rejection for autonomous acoustic navigation," in *Proc. IEEE Int. Conf. Robot. Autom.*, Apr. 1996, pp. 2174–2181.

[26] G. Agamennoni, J. I. Nieto, and E. M. Nebot, "An outlier-robust Kalman filter," in *Proc. IEEE Int. Conf. Robot. Autom. (ICRA)*, May 2011, pp. 1551–1558.

[27] T. W. Vaneck, C. D. Rodriguez-ortiz, M. C. Schmidt, and J. E. Manley, "Automated bathymetry using an autonomous surface craft," *Navigation*, vol. 43, no. 4, pp. 407–419, 1996.

[28] R. J. Meinhold and N. D. Singpurwalla, "Robustification of Kalman filter models," *J. Amer. Statist. Assoc.*, vol. 84, no. 406, pp. 479–486, Jun. 1989.

[29] F. J. Girón and J. C. Rojano, "Bayesian Kalman filtering with elliptically contoured errors," *Biometrika*, vol. 81, no. 2, pp. 390–395, 1994.

[30] G. Agamennoni, J. I. Nieto, and E. M. Nebot, "Approximate inference in state-space models with heavy-tailed noise," *IEEE Trans. Signal Process.*, vol. 60, no. 10, pp. 5024–5037, Oct. 2012.

[31] H. Nurminen, T. Ardeshiri, R. Piche, and F. Gustafsson, "Robust inference for state-space models with skewed measurement noise," *IEEE Signal Process. Lett.*, vol. 22, no. 11, pp. 1898–1902, Nov. 2015.
[32] D. Xu, C. Shen, and F. Shen, "A robust particle filtering algorithm with non-Gaussian measurement noise using student-t distribution," *IEEE Signal Process. Lett.*, vol. 21, no. 1, pp. 30–34, Jan. 2014.
[33] R. Pichě, S. Särkkä, and J. Hartikainen, "Recursive outlier-robust filtering and smoothing for nonlinear systems using the multivariate student-t distribution," in *Proc. IEEE Int. Workshop Mach. Learn. Signal Process.*, Sep. 2012, pp. 1–6.
[34] M. Roth, E. Özkan, and F. Gustafsson, "A Student's t filter for heavy tailed process and measurement noise," in *Proc. IEEE Int. Conf. Acoust., Speech Signal Process.*, May 2013, pp. 5770–5774.
[35] Y. Huang, Y. Zhang, N. Li, S. M. Naqvi, and J. Chambers, "A robust Student's t based cubature filter," in *Proc. Int. Conf. Inf. Fusion (FUSION)*, Jul. 2016, pp. 9–16.
[36] Y. Huang, Y. Zhang, N. Li, and J. Chambers, "A robust Gaussian approximate fixed-interval smoother for nonlinear systems with heavy-tailed process and measurement noises," *IEEE Signal Process. Lett.*, vol. 23, no. 4, pp. 468–472, Apr. 2016.
[37] Y. Huang, Y. Zhang, N. Li, and J. Chambers, "Robust Student's t based nonlinear filter and smoother," *IEEE Trans. Aerosp. Electron. Syst.*, vol. 52, no. 5, pp. 2586–2596, Oct. 2016.
[38] J.-B. Lacambre, M. Narozny, and J.-M. Louge, "Limitations of the unscented Kalman filter for the attitude determination on an inertial navigation system," in *Proc. IEEE Digit. Signal Process. Signal Process. Edu. Meeting (DSP/SPE)*, Aug. 2013, pp. 187–192.
[39] Fan. (2003). *The Introduction of PHINS*. [Online]. Available: http://www.globalspec.com/industrial-directory/inertial_navigation_unit
[40] G. Papadopoulos, M. F. Fallon, J. J. Leonard, and N. M. Patrikalakis, "Cooperative localization of marine vehicles using nonlinear state estimation," in *Proc. IEEE/RSJ Int. Conf. Intell. Robots Syst. (IROS)*, Oct. 2010, pp. 4874–4879.
[41] S. Kotz and S. Nadarajah, *Multivariate T-Distributions and Their Applications*. Cambridge, U.K.: Cambridge Univ. Press, 2004.
[42] C. M. Bishop, *Pattern Recognition and Machine Learning*. New York, NY, USA: Elsevier, 2006.
[43] G. Kurz, F. Pfaff, and U. D. Hanebeck, "Kullback-leibler divergence and moment matching for hyperspherical probability distributions," in *Proc. Int. Conf. Inf. Fusion (FUSION)*, Jul. 2016, pp. 2087–2094.
[44] F. M. Mirzaei and S. I. Roumeliotis, "A Kalman filter-based algorithm for IMU-camera calibration: Observability analysis and performance evaluation," *IEEE Trans. Robot.*, vol. 24, no. 5, pp. 1143–1156, Oct. 2008.
[45] B. Li, "Robust particle filter by dynamic averaging of multiple noise models," in *Proc. IEEE Int. Conf. Acoust., Speech Signal Process.*, Mar. 2017, pp. 4034–4038.
[46] T. Kailath, A. H. Sayed, and B. Hassibi, *Linear Estimation*. Englewood Cliffs, NJ, USA: Prentice-Hall, 2000.

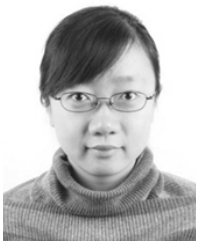

Qian Li received the M.S. degree from the Department of Aerospace Science and Technology, Shanghai Jiao Tong University, Shanghai, China, in 2010, and the Ph.D. degree from the Department of Automation, Harbin Engineering University, Harbin, China, in 2014.

From 2016 to 2017, she was an Academic Visitor with the School of Engineering, Newcastle University, Newcastle upon Tyne, U.K. She is currently a Lecturer with the Department of Electrical Engineering and Automation, Harbin Institute of Technology, Harbin. Her current research interests include information fusion and their applications in navigation technology, such as inertial navigation and integrated navigation.

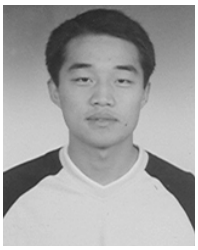

Yueyang Ben received the Ph.D. degree in precision instruments and mechanology from the Department of Automation, Harbin Engineering University, Harbin, China, in 2008.

Since 2005, he has been involved in the development of the fiber-gyro SINS for nautical navigation. He is currently an Associate Professor with the Department of Automation, Harbin Engineering University. His current research interests include strapdown algorithms, estimation theory and application in SINS initial alignment, and data processing.

Syed Mohsen Naqvi (S'07–M'10–SM'15) received the Ph.D. degree in signal processing from Loughborough University, Loughborough, U.K., in 2009.

From 2002 to 2005, he was with the National Engineering and Scientific Commission, Islamabad, Pakistan. From 2009 to 2015, he was a Post-Doctoral Research Associate with EPSRC U.K.-funded projects and an REF Lecturer with Loughborough University. He is currently a Lecturer of signal and information processing with the School of Engineering, Newcastle University, Newcastle upon Tyne, U.K. He has authored or co-authored more than 90 publications with the main focus of his research being on multimodal (audio–video) signal and information processing. He has successfully (co)-supervised 25 Ph.D. and M.Sc. students and is (co)-supervising 8 Ph.D. students. He organized special sessions on multitarget tracking in FUSION 2013 and 2014, delivered seminars. His current research interests include multimodal processing for human behavior analysis, multitarget tracking, and source separation, all for machine learning.

Dr. Naqvi is a fellow of the Higher Education Academy U.K., a member of the University Defense Research Collaboration in Signal Processing, and a member of the International Society of Information Fusion. He was a Speaker at UDRC Summer Schools from 2015 to 2017.

Jeffrey A. Neasham received the B.Eng. degree in electronic engineering from Newcastle University, Newcastle upon Tyne, U.K., in 1994.

He joined Newcastle University, as a Research Associate, where he was involved in research and commercial product development in underwater acoustic communication, sonar imaging, and wireless sensor networks. He is currently a Senior Lecturer in communications and signal processing with the School of Electrical and Electronic Engineering, Newcastle University. He has authored or co-authored over 80 conference and journal publications and his work on underwater modem design has been commercialized by three U.K. companies. His current research interests include underwater acoustic signal processing and device design, wireless communication networks, and biomedical instrumentation.

Jonathon A. Chambers (S'83–M'90–SM'98–F'11) received the Ph.D. and D.Sc. degrees in signal processing from the Imperial College of Science, Technology and Medicine (Imperial College London), London, U.K., in 1990 and 2014, respectively.

From 1991 to 1994, he was a Research Scientist with the Schlumberger Cambridge Research Center, Cambridge, U.K. In 1994, he joined Imperial College London, as a Lecturer in signal processing and was promoted to Reader (Associate Professor) in 1998. From 2001 to 2004, he was the Director of the Center for Digital Signal Processing and a Professor of signal processing with the Division of Engineering, King's College London, London, where he is currently a Visiting Professor. From 2004 to 2007, he was a Cardiff Professorial Research Fellow with the School of Engineering, Cardiff University, Cardiff, U.K. From 2007 to 2014, he led the Advanced Signal Processing Group, School of Electronic, Electrical and Systems Engineering, Loughborough University, Loughborough, U.K., where is currently a Visiting Professor. In 2015 and 2017, he joined the School of Electrical and Electronic Engineering and the School of Engineering, Newcastle University, Newcastle upon Tyne, U.K., where he was a Professor of signal and information processing and the Head of the Intelligent Sensing and Communications Group, where he is currently a Visiting Professor. Since 2017, he has been the Head of the Engineering Department, University of Leicester, Leicester, U.K. He is also an International Honorary Dean and a Guest Professor with the Department of Automation, Harbin Engineering University, Harbin, China. He has advised 80 researchers through to Ph.D. graduation. He has authored or co-authored more than 500 conference proceedings and journal articles, many of which are in the IEEE journals. His current research interests include adaptive signal processing and machine learning and their application in communications, defense, and navigation systems.

Dr. Chambers is a fellow of the Royal Academy of Engineering, London, U.K., the Institution of Engineering and Technology, Stevenage, U.K., and the Institute of Mathematics and its Applications, Southend-on-Sea, U.K. He was a Technical Program Co-Chair for the 36th IEEE International Conference on Acoustics, Speech, and Signal Processing (ICASSP), Prague, Czech Republic. He is serving on the organizing committees of ICASSP 2019 Brighton, U.K., and ICASSP 2022, Singapore. He has served on the IEEE Signal Processing Theory and Methods Technical Committee for six years, the IEEE Signal Processing Society Awards Board for three years, and the Jack Kilby Medal Committee for three years.